British Geological Survey
NATURAL ENVIRONMENT RESEARCH COUNCIL

Laboratory study examining permeability evolution along an isotropic unloading stress path

Chemical and Biological Hazards Programme

Open Report OR/07/016

BRITISH GEOLOGICAL SURVEY

CHEMICAL AND BIOLOGICAL HAZARDS PROGRAMME

OPEN REPORT OR/07/016

Laboratory study examining permeability evolution along an isotropic unloading stress path

DJ Birchall, JF Harrington, DJ Noy and RJ Cuss

Keywords

Opalinus clay, permeability, isotropic, stress path, specific storage, volumetric strain, bulk modulus, Young's modulus, compressibility, unloading, relaxation.

Front cover

Photo of test specimen following decommissioning of the apparatus

Bibliographical reference

DJ Birchall, JF Harrington, DJ Noy and RJ Cuss. 2008. Laboratory study examining permeability evolution along an isotropic unloading stress path. *British Geological Survey Open Report*, OR/07/016. 33pp.

Keyworth, Nottingham British Geological Survey 2008

BRITISH GEOLOGICAL SURVEY

The full range of our publications is available from BGS shops at Nottingham, Edinburgh, London and Cardiff (Welsh publications only) see contact details below or shop online at www.geologyshop.com

The London Information Office also maintains a reference collection of BGS publications, including maps, for consultation.

We publish an annual catalogue of our maps and other publications; this catalogue is available online or from any of the BGS shops.

The British Geological Survey carries out the geological survey of Great Britain and Northern Ireland (the latter as an agency service for the government of Northern Ireland), and of the surrounding continental shelf, as well as basic research projects. It also undertakes programmes of technical aid in geology in developing countries.

The British Geological Survey is a component body of the Natural Environment Research Council.

British Geological Survey offices

BGS Central Enquiries Desk
Tel 0115 936 3143 Fax 0115 936 3276
email enquires@bgs.ac.uk

Kingsley Dunham Centre, Keyworth, Nottingham NG12 5GG
Tel 0115 936 3241 Fax 0115 936 3488
email sales@bgs.ac.uk

Murchison House, West Mains Road, Edinburgh EH9 3LA
Tel 0131 667 1000 Fax 0131 668 2683
email scotsales@bgs.ac.uk

London Information Office at the Natural History Museum (Earth Galleries), Exhibition Road, South Kensington, London SW7 2DE
Tel 020 7589 4090 Fax 020 7584 8270
Tel 020 7942 5344/45 email bgslondon@bgs.ac.uk

Columbus House, Greenmeadow Springs, Tongwynlais, Cardiff CF15 7NE
Tel 029 2052 1962 Fax 029 2052 1963

Forde House, Park Five Business Centre, Harrier Way, Sowton EX2 7HU
Tel 01392 445271 Fax 01392 445371

Maclean Building, Crowmarsh Gifford, Wallingford OX10 8BB
Tel 01491 838800 Fax 01491 692345

Geological Survey of Northern Ireland, Colby House, Stranmillis Court, Belfast BT9 5BF
Tel 028 9038 8462 Fax 028 9038 8461

www.bgs.ac.uk/gsni/

Parent Body

Natural Environment Research Council, Polaris House, North Star Avenue, Swindon SN2 1EU
Tel 01793 411500 Fax 01793 411501
www.nerc.ac.uk

Website www.bgs.ac.uk
Shop online at www.geologyshop.com

Acknowledgements

This study was undertaken using the facilities of the BGS Transport Properties Research Laboratory (TPRL). Funding for the study was provided by the Geosphere Containment Project (part of the BGS core strategic programme) and the Swiss radioactive waste management operator, Nagra.

The authors would like to thank the following for their contribution during the review process:

Peter Hobbs

Joanna Thomas

Ben Klinck

Contents

FIGURES

TABLES

Executive summary

A small experimental study sponsored by the British Geological Survey (aligned to the Geosphere Containment Project) and the Mont Terri Consortium (as part of the HA experimental programme) was undertaken by the Transport Properties Research Laboratory (TPRL). The objective of the work was to provide information on the evolution of intrinsic permeability and the stress-dependent specific storage of an Opalinus Clay specimen subject to an isotropic unloading stress history.

Isotropic effective stress was reduced in a step wise manner on a specimen of Opalinus Clay subject to a constant hydraulic gradient. Permeability values were found to be in the range 3.8 to 9.5 x 10^{-21} m^2 at average effective stresses of 3.25 to 0.40 MPa respectively, with permeability significantly increasing when effective stress declined to below around 1.0 MPa. However, this study clearly shows that on the scale of this experiment, the specimen continues to exhibit very low permeability.

Storage values for the stress regime imposed during this study were found to range from 3.8 to 46.7 x10^{-5} m^{-1}, exhibiting a general trend of increasing storage with decreasing effective stress.

The relationship between void ratio and logarithm of effective stress is reasonably linear for the stress regime of the test indicating the specimen exhibits soil-like behaviour. Evidence suggests that the locus in void ratio-effective stress space corresponds to the rebound-reconsolidation line of theoretical soil mechanics. The general trend of increasing material compressibility and decreasing bulk modulus are symptomatic of an increase in specimen volume due to swelling of the clay during stress unloading.

Values of Young's modulus based on analysis of the unloading data are generally lower than those derived from numerical modelling of the data. However, both determinants exhibit a general decreasing trend as average effective stress declines. The combination of low modulus values and the inability of the numerical model to fit all the data simultaneously, strongly suggests that the specimen is exhibiting a form of visco-plastic deformation during the unloading process.

1 Introduction

A small experimental study sponsored by the British Geological Survey (aligned to the Geosphere Containment Project) and the Mont Terri Consortium (as part of the HA experimental programme) was undertaken by the Transport Properties Research Laboratory (TPRL). The objective of the work was to provide information on the evolution of intrinsic permeability and the stress-dependent specific storage (Wood, 1990; Horseman et al., 1993) of an Opalinus Clay (OPA) specimen subject to an isotropic unloading stress history. Data from this experiment can be used to assist in the assessment of the long-term evolution of a mudrock geological barrier (Horseman, 2001).

The equation of porewater flow is obtained by combining Darcy's Law with the equation of fluid mass conservation to give (de Marsily, 1986):

$$S_s \frac{\partial h}{\partial t} = \nabla . \left(\frac{k_i \rho_w g}{\mu_w} \nabla h \right) + Q \tag{1}$$

where S_s is the specific storage (m^{-1}), k_i is the intrinsic permeability (m^2), ρ_w is the density of water ($kg.m^{-3}$), g is the acceleration due to gravity ($m.s^{-2}$), μ_w is the viscosity of water (Pa.s), h is the hydraulic head (m) and Q is the rate of fluid volume injection per unit volume of porous medium (s^{-1}). This equation is solved here by the finite element method for an axisymmetric two dimensional domain subject to specified head and specified flow boundary conditions. Hydraulic head is related to the pore-water pressure by $p_w = \rho_w g h$.

In order to model the consolidation tests it is necessary to couple the porewater flow equation to equations for the stress-strain relationships. The porewater equation for this takes the form Huyakorn and Pinder (1983):

$$\nabla . (K \nabla h) = \phi \beta \rho_w g \frac{\partial h}{\partial t} + \frac{\partial}{\partial t} (\nabla . \mathbf{u}) \tag{2}$$

where ϕ is the porosity, β is the fluid compressibility (Pa^{-1}), and $\mathbf{u}$ is the vector of solid phase displacements (m). For the case of elastic plane strain, the equations for the displacements are

$$\left(\frac{E}{2(1+\nu)} \right) \frac{\partial^2 u_i}{\partial x_j \partial x_j} + \left(\frac{E}{2(1+\nu)(1-2\nu)} \right) \frac{\partial^2 u_j}{\partial x_i \partial x_j} - \rho_w g \frac{\partial h}{\partial x_i} = 0 \qquad (i=1,2) \tag{3}$$

where summation over repeated index j is assumed. Here E is the Young's modulus (Pa) and ν is the Poisson's ratio. Equations (2) and (3) are solved using the finite element code STAFAN (Intera, 1983). While this analysis assumes purely elastic behaviour, it provides an initial framework for the interpretation of the experimental data. To accurately model deformation processes in argillaceous materials requires the development of time dependent non-linear stress-strain models (i.e. visco-plastic) which is beyond the remit of this programme of work.

2 Apparatus

The basic permeameter consists of five main components: (1) a specimen assembly, (2) a 70 MPa rated pressure vessel and associated confining pressure system, (3) a fluid injection system, (4) a backpressure system, and (5) a PC-based data acquisition system. The specimen is subject to an isotropic confining stress. A novel feature of the apparatus is the use of porous annular guard-ring filters around the inflow and outflow filters. The pressures in these two guard-rings can be independently monitored. The advantages of the guard-ring approach are: (a) pore pressure evolution can be studied, (b) hydraulic anisotropy can be quantified in a single test, (c) a check can be made of flow symmetry in the specimen, (d) excess gas pressure at gas entry can be accurately determined, and (e) uncertainties associated with possible sheath leakage can be eliminated from data interpretation.

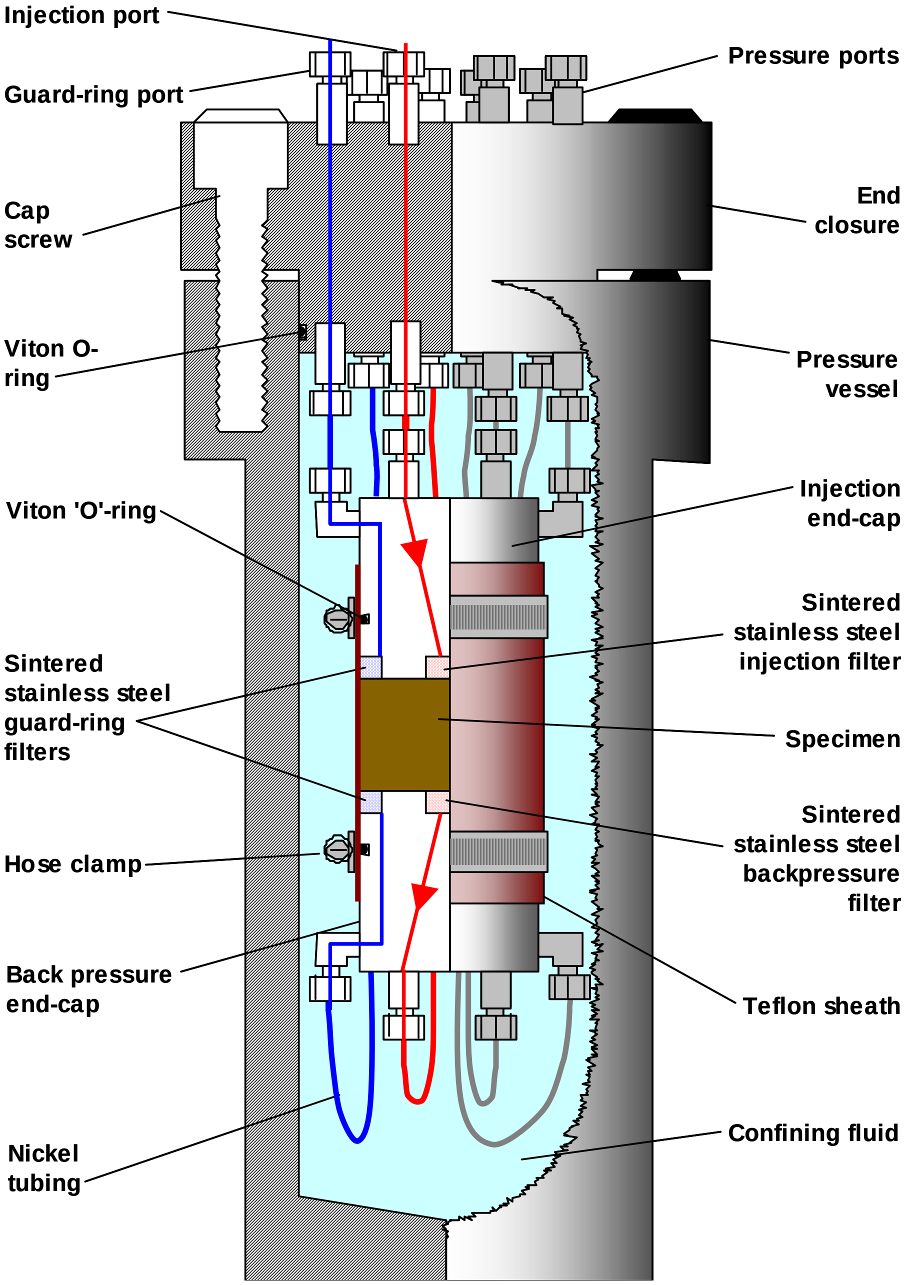

Figure 2-1 Cut-away diagram of the pressure vessel and sample assembly for the BGS guard-ring permeameter.

The test specimen is sandwiched between two stainless steel end-caps and jacketed in heat-shrink Teflon to exclude confining fluid. Jubilee hose clamps and copper shims compress the Teflon against a Viton "O"-ring in each end-cap to provide a leak-tight seal. The inlet and outlet zones for water or gas flow through the specimen are provided by porous filter discs 20 mm in diameter which are recessed into the bearing surface of the end-caps (Figure 2-1). These act as either source or sink for the injection of test permeants. Annular guard-ring filters with an internal diameter of 44 mm and an external diameter of 50 mm are recessed into the end-caps so that they completely encircle the inlet and outlet filters. A seal between the guard-ring and source/sink filters is achieved through the application of the confining stress, compressing the carefully machined surface of each platen against the clay. During hydraulic measurements, all the filters are saturated with an synthetic porewater solution.

Volumetric flow rates are controlled or monitored using a pair of ISCO-500, Series D, syringe pumps operated from a single digital control unit. The position of each pump piston is determined by an optically encoded disc graduated in segments equivalent to a change in volume of 31.71 nL. Movement of the pump piston is controlled by a micro-processor which continuously monitors and adjusts the rate of rotation of the encoded disc using a DC-motor connected to the piston assembly via a geared worm drive. This allows each pump to operate in either constant pressure or continuous flow modes. A programme written in LabVIEW™ elicits data from the pump at pre-set time intervals. Testing is performed in an air-conditioned laboratory at a nominal temperature of 20 ºC. A typical test history comprises a sequence of test stages, each designed to examine a particular system response, as described in Section 4.

2.1 CALIBRATION

All pressure sensors were calibrated against laboratory standards by applying incremental steps in pressure, from atmospheric to a pre-determined maximum value. This was followed by a descending history to quantify any hysteresis. Least-squares fits were calculated and the regression parameters used to correct raw data.

On decommissioning of the apparatus a small drift in the pump transducer values for both injection and backpressure systems was observed (0.10 MPa and 0.14 MPa respectively). Inspection of the guard-ring data indicates that the drift was not present for most of the test history. Data suggests that an initial drift occurred during test stage [7] following an interruption in the electrical power supply to the laboratory. The remaining drift in sensor output would seem to have occurred during the final decommissioning process and will therefore not have a detrimental affect on the results of this study.

3 Test material

The Opalinus Clay is a Jurassic (Aalenian) marine clayshale. The formation, named after the ammonite *Leioceras opalinum*, consists of indurated dark grey micaceous claystones (shales) that are subdivided into several lithostratigraphic units. Some of them contain thin sandy lenses, limestone concretions, or siderite nodules. The clay-mineral content ranges from 40-80 wt% (9-29% illite, 3-10% chlorite, 6-20% kaolinite, and 4-12% illite/smectite mixed layers in the ratio 70/30). Other minerals are quartz (15-30%), calcite (6-40%), siderite (2-3%), ankerite (0-3%), feldspars (1-7 %), pyrite (1-3 %), and organic carbon (<1%). The total water content ranges from 4-19% (Gautschi, 2001).

Preserved core samples of Opalinus Clay from the Mont Terri Underground Research Laboratory were delivered to BGS. A cylindrical test specimen was prepared from core taken from borehole BHA-5 (interval 70-80cm) by a combination of dry core-drilling, slicing and surface grinding (Figure 3-1). Table 3-1 shows the basic physical properties of the specimens compared to an average of the data presented by Horseman et al. (2007). Porosity and degree of saturation are based on a measured grain density of 2.695 $Mg.m^{-3}$. While there is general agreement between the pre-test values reported by Horseman et al. and those from this study, it is clear that specimen OPA-3 exhibits a marginally lower porosity and commensurately higher densities, suggesting a slightly higher degree of compaction.

Given the somewhat irregular shape of the specimen upon removal from the apparatus, post-test measurements (in particular saturation), which are extremely sensitive to minor changes in specimen dimension, should be treated with caution. This issue will be discussed briefly in Section 6.

Specimen		Length (mm)	Diameter (mm)	Moisture content (%)	Porosity (%)	Bulk density $Kg.m^{-3}$	Dry density $Kg.m^{-3}$	Saturation (%)
OPA-3	Pre-test	29.5	49.9	5.5	13.8	2453	2324	93
	Post-test	29.6	50.1	7.1	15.0	2452	2290	108
Average	Pre-test	-	-	5.8	15.2	2412	2280	86

Table 3-1 Dimensions and properties of the test specimens based on a grain density for the mineral phases of 2695 $kg.m^{-3}$. Pre-test measurements of specimen length for OPA-3 are derived from an assumed bulk density determined from previous attempts to manufacture a test specimen using material recovered from the same core run.

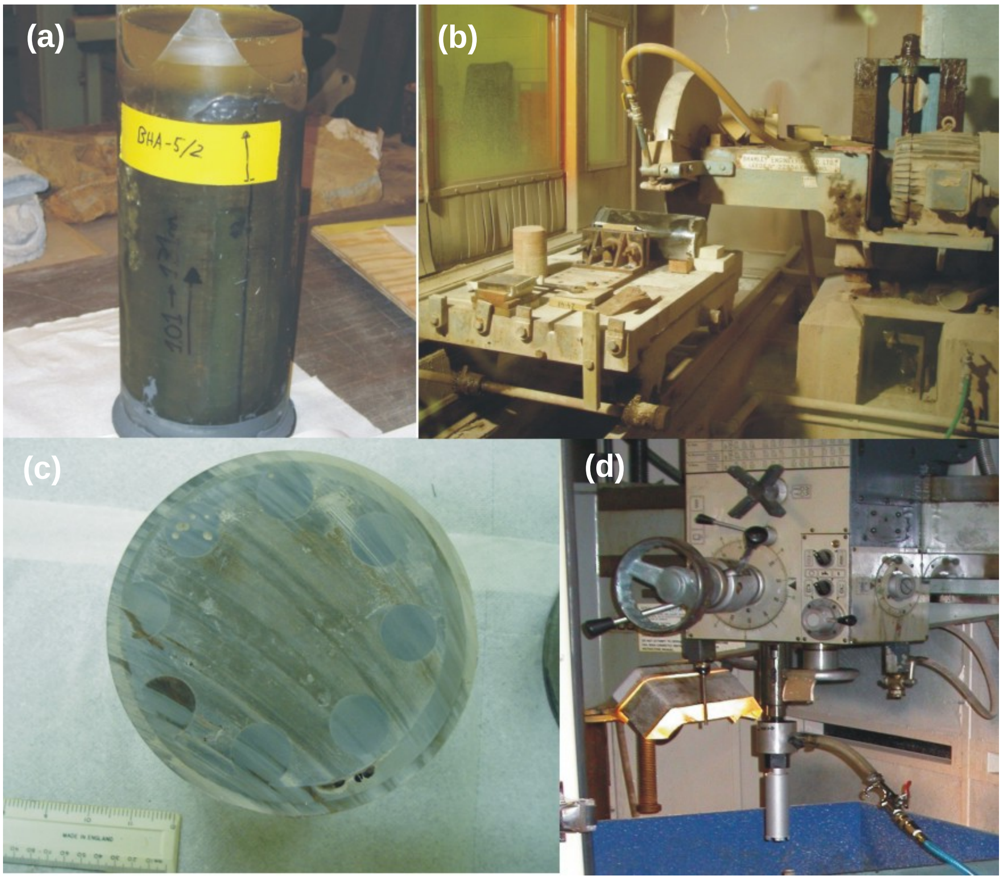

Figure 3-1 Manufacturing process for the test specimen; (a) intact core as received by BGS: (b) diamond saw used to section the core; (c) end view of core following sectioning showing resin impregnation as a result of coring during field sampling; (d) pillar drill used to diamond core sectioned block.

4 Experimental procedure

In order to limit osmotic swelling of the specimen, a synthetic porewater solution was prepared for use as the backpressuring fluid and permeant in the hydraulic test stages. Guided by hydrochemical studies of the Opalinus Clay for the Mt. Terri Project, a stock solution was prepared containing 7.598 $g.l^{-1}$ NaCl, 0.231 $g.l^{-1}$ KCl, 0.496 $g.l^{-1}$ $MgCl_2$, 0.803 $g.l^{-1}$ $CaCl_2$, 1.420 $g.l^{-1}$ Na_2SO_4 and 0.033 $g.l^{-1}$ Na_2CO_3 (Pearson et al., 1999). *In situ* (isotropic) confining stress data was provided by Nagra with the initial confining stress nominally set to 4.5 MPa with a backpressure of 1.0 MPa.

The experimental history comprises a sequence of test stages (Table 4-1). During an equilibrium (EQ) stage, the specimen is exposed to synthetic porewater solution with backpressure held constant. In a constant pressure hydraulic stage (CPH) a fixed pressure gradient is applied across the specimen. These stages are used to provide data in order to evaluate the intrinsic permeability and specific storage of the specimen for a given stress regime. During an unloading (UN) stage, the confining pressure acting on the specimen is incrementally reduced (the hydraulic gradient imposed during test stage [2] remains constant). By monitoring flux in to and out of the specimen it is possible to calculate both the volumetric strain associated with the reduction in confining stress and the change in intrinsic permeability.

Stage number	**0**	**1**	**2**	**3**	**4a**	**4b**	**5**	**6**	**7**
Type of test	EQ	CPH	CPH	UN	UN	UN	UN	UN	UN
Confining pressure	4.44	4.44	4.45	3.83	3.19	3.18	2.54	1.90	1.71
Injection pressure	1.01	1.37	1.62	1.62	1.62	1.62	1.62	1.62	1.62
Backpressure	1.01	1.01	1.01	1.01	1.01	1.01	1.01	1.01	1.01
Ave, effective stress	3.46	3.25	3.14	2.51	1.87	1.86	1.22	0.59	0.40

Table 4-1 Initial experimental history for specimen NS-S2. CO = consolidation stage; EQ = equilibrium stage; CPH = constant pressure hydraulic stage; UN = unloading stage.

5 Test history

The test specimen was initially subject to an isotropic confining stress of 4.5MPa for a period of around 20 days with injection and back pressure filters held constant at 1.0 MPa. During this period a net inflow of fluid (~1.2 ml) was observed (Figure 5-1), associated with the resaturation and equilibration of the specimen under the applied stress regime. Scoping calculations based on the pre-test geotechnical properties (Table 3-1) indicate the observed flux is commensurate with saturation of the specimen (i.e. S_w~100% at the start of hydraulic testing).

The time scales in the plots below start with t=0 set to the end of the preliminary stage [0]. The injection pressure was then raised to 1.37 MPa for 8 days and raised again to 1.62 MPa, at which pressure it was maintained for the rest of the test. The confining pressure was then reduced in a series of steps as shown in Figure 5-2. Figures 5-3 and 5-4 show the pressures on the injection and back pressure filters and guard rings, and the flow rates observed at the inlet and sink filters. It can be seen that the guard ring filters were not isolated from their respective end-piece filters until the start of test stage [4b] at around 73 days into the test. After this occurred, the injection guard ring pressure dropped by about 100 kPa, but the back pressure guard ring only rose by about 35 kPa and in fact apparently remained at a lower pressure than the back pressure filter itself. These observations can be explained by bypass flow across the face of the downstream platen and a small error in the initial calibration of the guard-ring pressure devices. As such no further consideration of the guard ring data is made in this report.

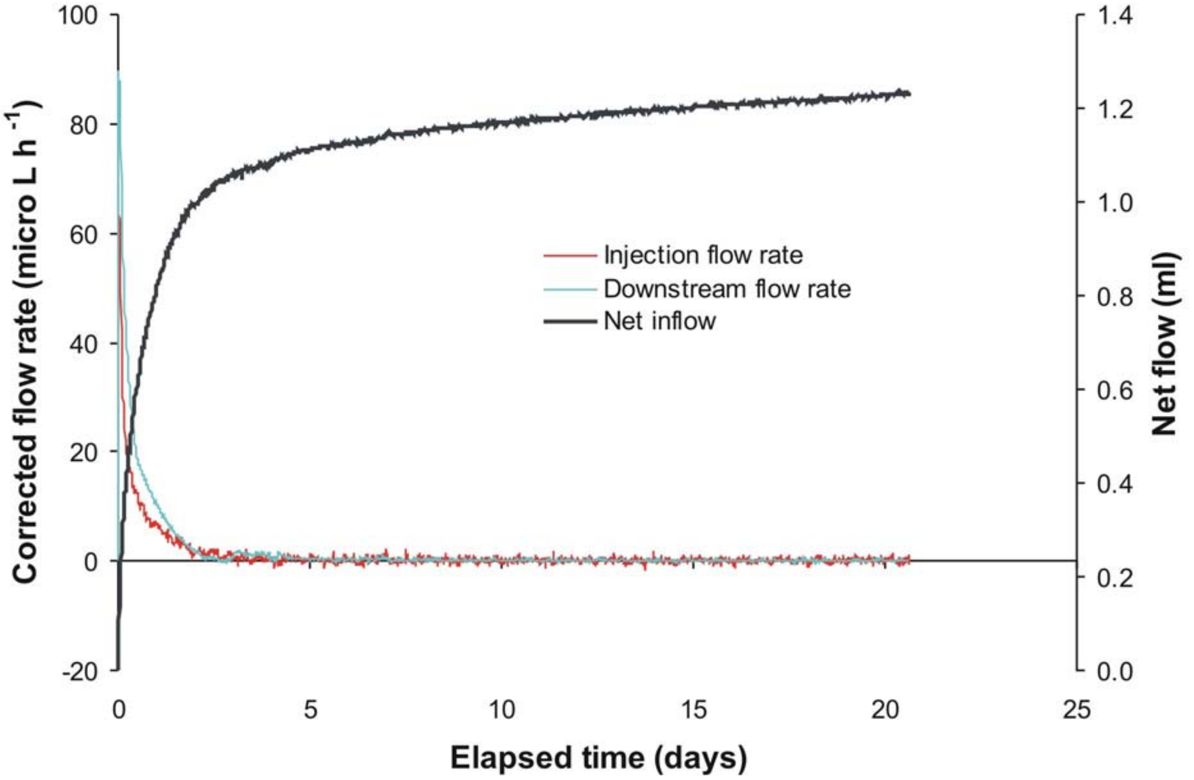

Figure 5-1 Flow into the specimen during test stage [0] associated with resaturation of the specimen. Corrected fluxes have been used to compensate for a small leak from the backpressure pump during the first 4 days of testing.

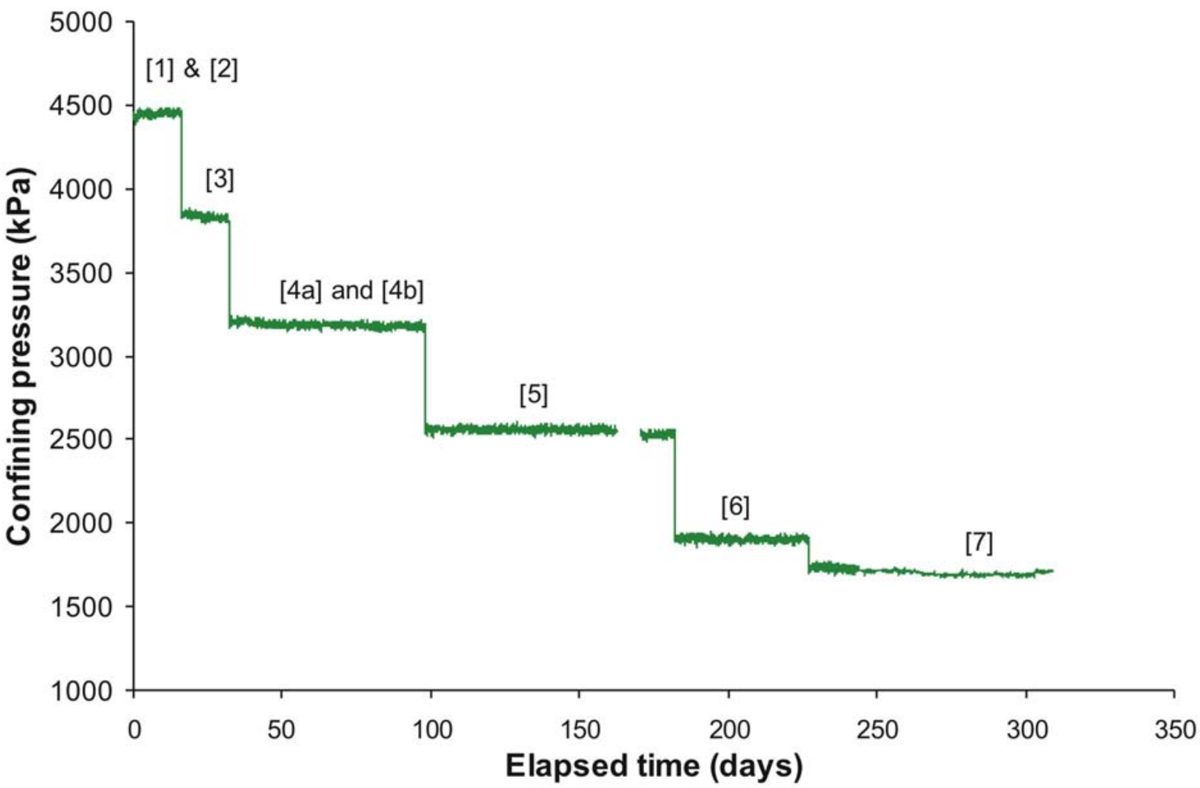

Figure 5-2 Confining pressure history during the test.

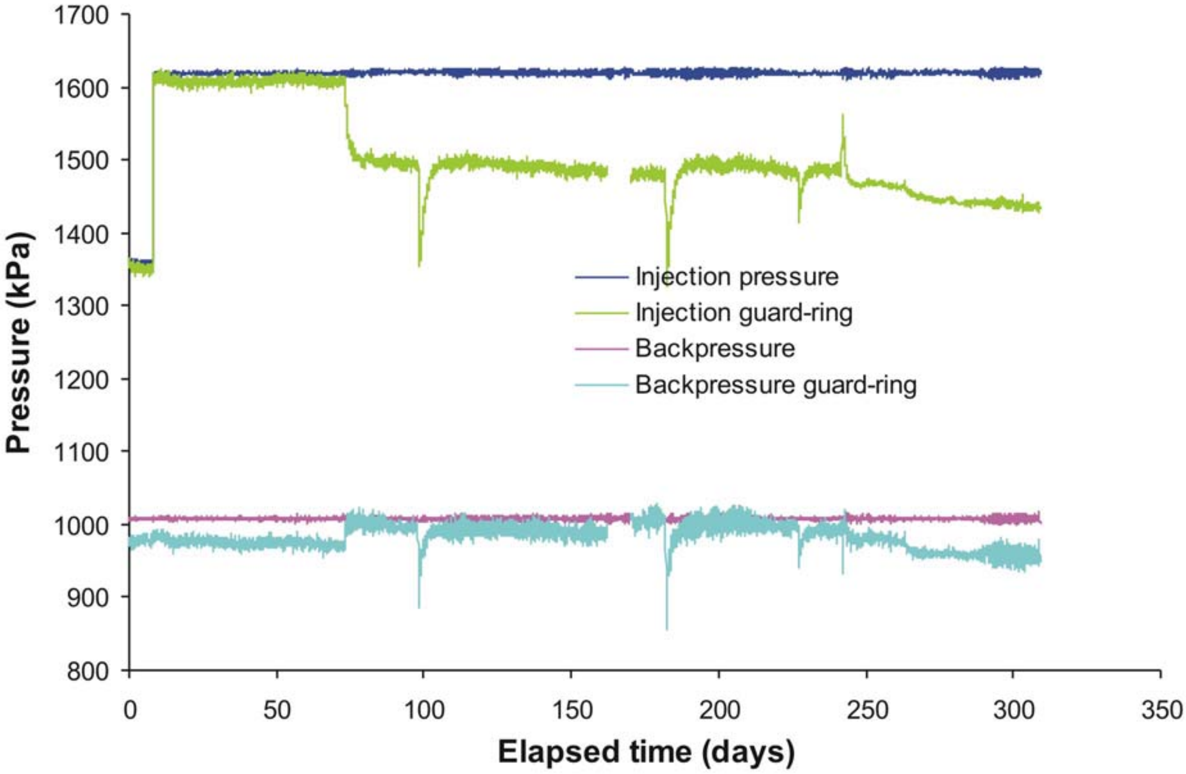

Figure 5-3 Pressures at injection and backpressure filters and guard rings.

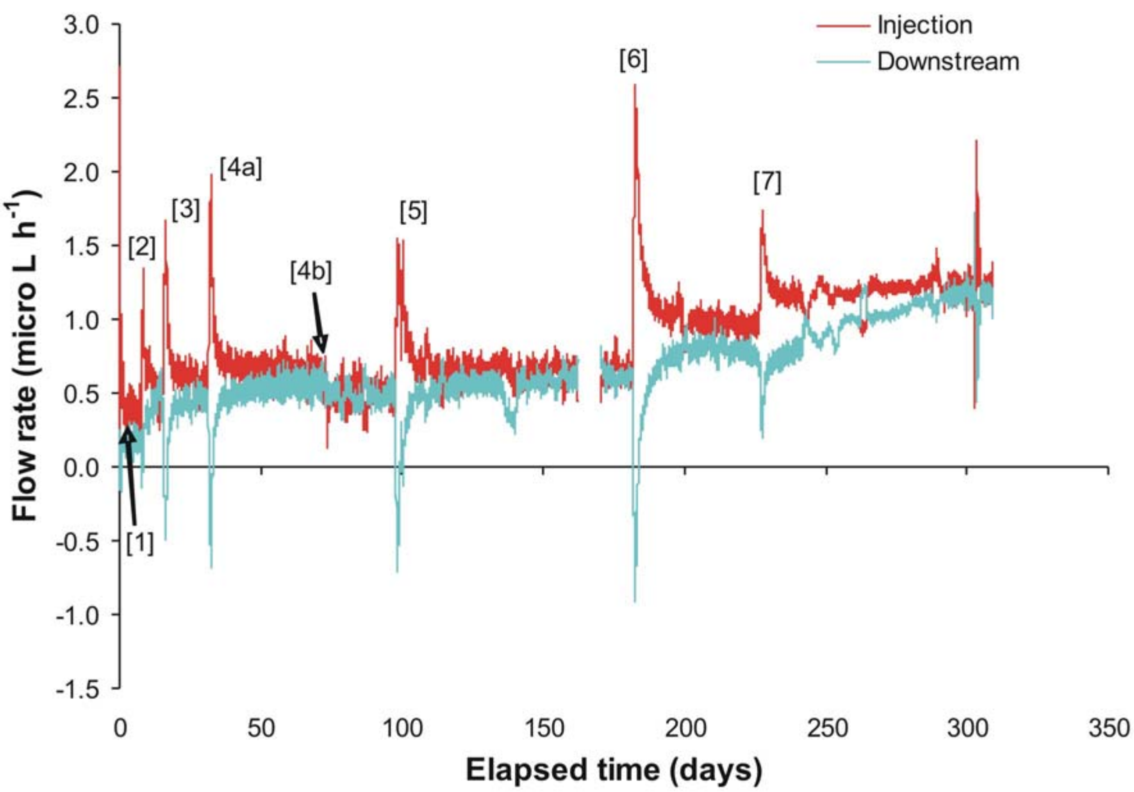

Figure 5-4 Flow rates at injection and backpressure filters.

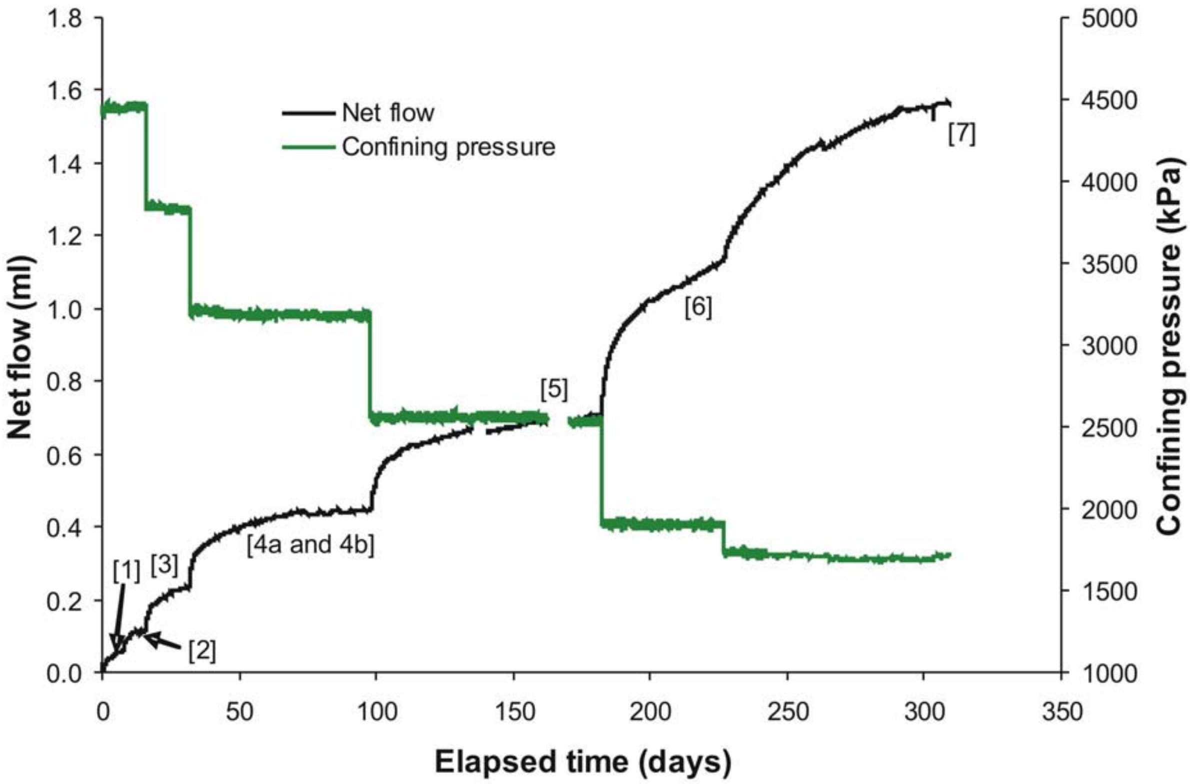

Figure 5-5 Plot of net flow into the sample during the test.

The flow rate curves show distinctive spikes at each change of either the injection or confining pressures, with the inflows and outflows largely converging again about 10 days after each boundary condition change. During the middle stages of the test the inflows and outflows converge on a rate of about 0.6 $\mu l.h^{-1}$, (Figure 5-4). The data from around 162 to 170 days has been removed from all plots due to fluctuations in output signals caused by a temporary failure of the air conditioning system. In test stage [6], the two flow rate curves do not converge fully and it would appear that the stage was terminated prematurely. In the final test stage [7], the flow rates appear to increase steadily with time. The fact that both flows converge at around 300 days indicates that this is a genuine effect and a true material response.

The final dataset available from the test for comparison with model output is the evolution of the net flow into the specimen, which is plotted in Figure 5-5. Here it can be seen that test stages ending at around 100 and 180 days, i.e. [4b] and [5], have levelled off to a relatively steady state, but the later stages do not reach such a clearly defined asymptote. This can be explained by time dependent swelling of the clay in the later stages of the experimental history.

6 Results

Figure 6-1 shows the standard geotechnical plot of void ratio against the logarithm of effective stress (Schofield and Wroth, 1968; Atkinson and Bransby, 1978). Examination of the data indicates the line is sensibly linear throughout the entire test history with only minor departures caused by the premature termination of specific tests stages, in particular stage [6]. The linear section of any part of a consolidation curve can be represented by the general relationship:

$$e = e_o - \alpha \ln\left(\frac{\sigma'}{\sigma_0'}\right) \qquad (4)$$

where -α is the slope, σ' is the effective stress acting on the specimen, and e_o is the void ratio intercept at an effective stress, σ_0', equal to 1.0 MPa. Values of void ratio and α are given in Table 6-1. Analysis of the consolidation transients indicates secondary consolidation (i.e. time-dependent volumetric creep of the fabric) still in progress at the end of some test stages. The superposition of the hydraulic and rheological responses will have a minor effect on the calculated consolidation parameters, but this is unavoidable given the practical constraints on test duration.

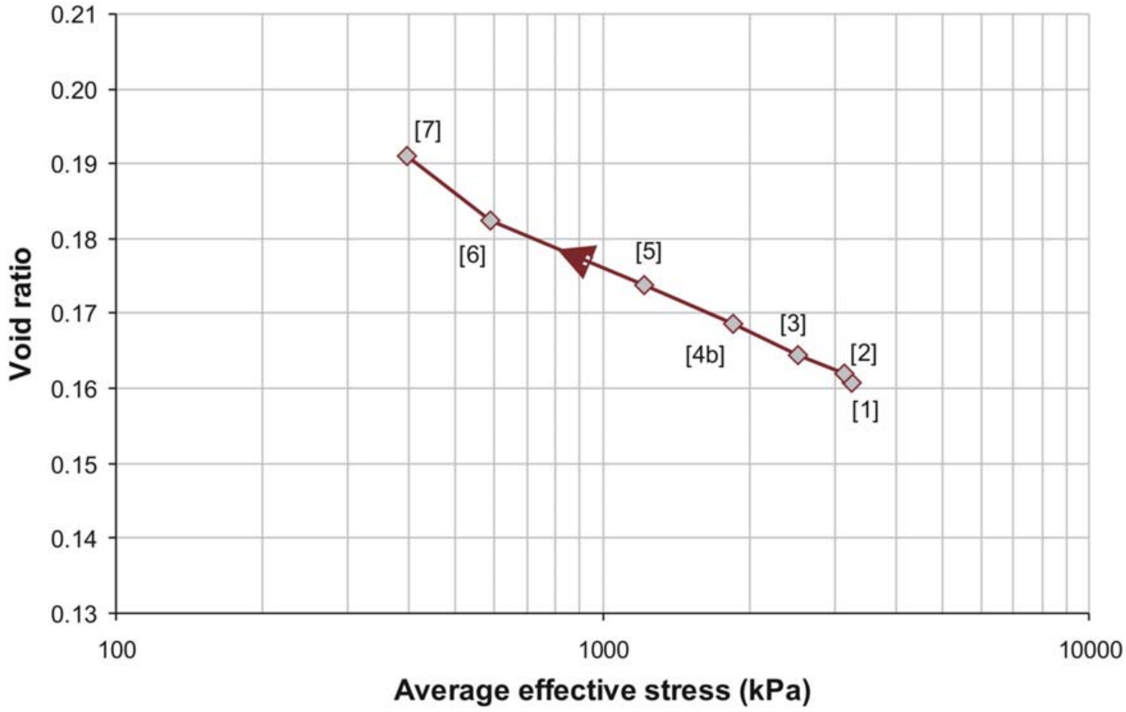

Figure 6-1 Void ratio against logarithm of effective stress for test stages [1] to [7].

Stage no.	Ave. effective stress (MPa)	Void ratio (at end of stage)	Gradient of slope α	Volumetric strain (%)	Drained compressibility $\beta/10^9$ (Pa^{-1})	Drained bulk modulus of relaxation[1] (MPa)
1	3.25	0.161	-	-0.11	-	-
2	3.14	0.162	0.061	-0.20	8.1	125
3	2.51	0.164	0.011	-0.41	3.4	291
4	1.86	0.168	0.013	-0.77	5.5	181
5	1.22	0.173	0.012	-1.23	7.1	140
6	0.59	0.181	0.011	-1.97	11.7	86
7	0.40	0.190	0.021	-2.72	39.9	25

Table 6-1 Unload data for test specimen. Negative volumetric strain indicates an increase in specimen volume.

[1] Bulk modulus is normally derived in a system where overall stress is increasing (loading) whereas this parameter is a bulk modulus derived during an overall reduction in stress (unloading). This should not be confused with a classic stress relaxation test where a specimen is driven to a specific load, the test paused and the deformation monitored.

Inspection of the unload data in Table 6-1 indicates a progressive increase in void ratio (i.e. specimen volume) as isotropic confining stress is reduced. The general trends of increasing material compressibility and decreasing bulk modulus are also symptomatic of an increase in specimen volume due to swelling of the clay during stress unloading. The values of bulk modulus (during stress reduction) quoted in Table 6-1 are extremely small and can be explained by non-elastic deformation (e.g. swelling). Alpha values from this study are in general agreement to those obtained by Horseman et al. (2005) for clay in the overconsolidated domain, suggesting quantitatively similar material behaviour.

Figure 6-2 shows the evolution in volumetric strain in response to the reduction in boundary stress. While some of the tests stages do not approach a well defined asymptote, the data clearly indicates that the amount of volumetric strain (swelling) per stage appears to increase as effective stress is reduced.

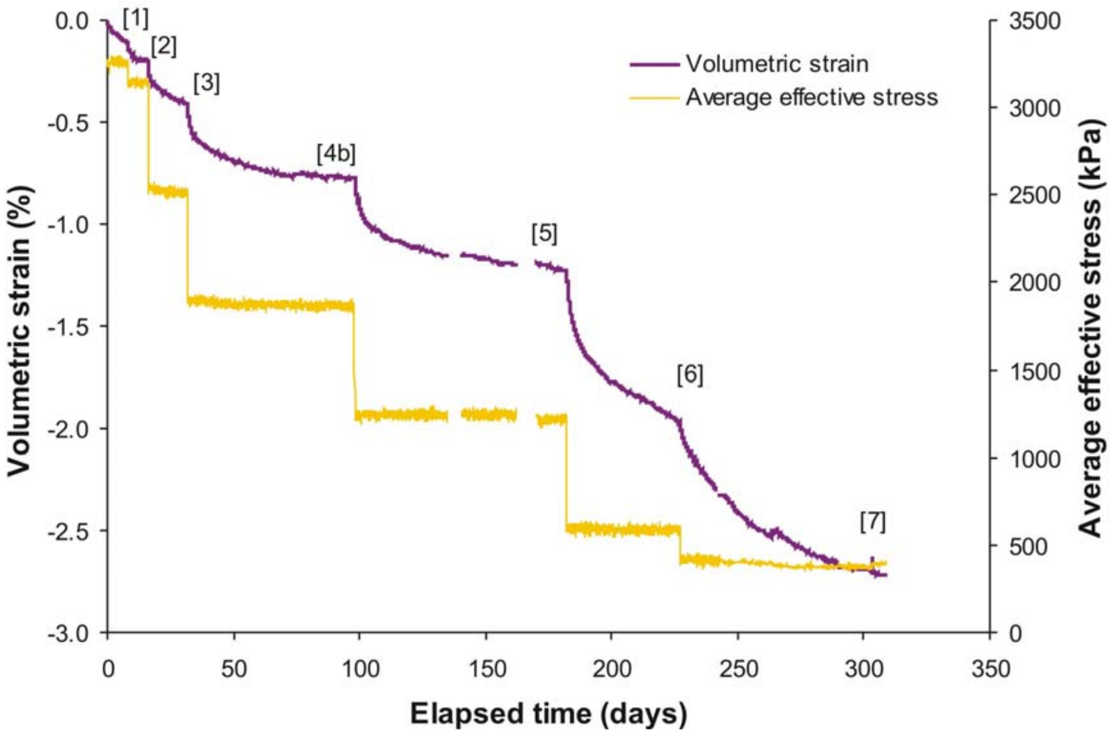

Figure 6-2 Evolution of volumetric strain and average effective stress during test stages [1] to [7] inclusive. The data clearly exhibits the specimen undergoing negative volumetric strain symptomatic of swelling of the specimen.

For an overconsolidated clay under an isotropic stress, the specific storage (m^{-1}) is given by:

$$S_s = \frac{\rho_w g}{1+e}\left[\frac{e}{K_w} + \frac{\kappa}{\sigma'}\right] \qquad (5)$$

where ρ_w is the density of water, K_w the bulk modulus of water and κ is a dimensionless parameter representing the gradient of the rebound-reconsolidation line in void ratio vs. effective stress space (Horseman and Harrington, 1994). Setting κ equal to the α parameter, an estimate for the specific storage for each unloading stage can be obtained (Table 6-2). Storage values calculated in this way are plotted against average effective stress, Figure 6-3, and show a general trend of increasing storage with decreasing effective stress. Storage values obtained in this way are significantly larger than those reported by Horseman et al. (2005). However, this can be readily explained by the stress dependency of the storage parameter and the low effective stresses imposed on the test specimen during this study.

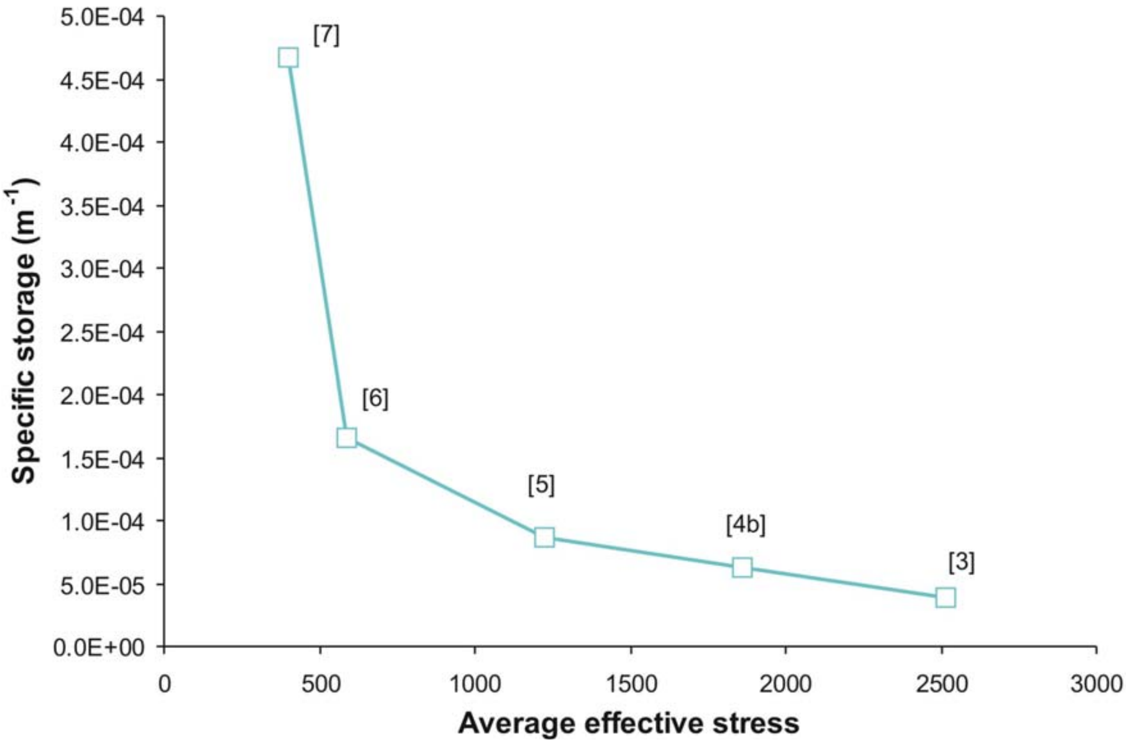

Figure 6-3 Specific storage against average effective stress for test stages [3] to [7] inclusive. Data from stage [2] has not been included due to the premature termination of the test stage [1] and the superposition of material responses.

The specific storage coefficient arises from skeletal deformation of the porous medium and can be related to Young's modulus. Assuming that the fluid compressibility is negligible and writing the solid compressibility in terms of Young's modulus, E, and Poisson's ratio, ν, (de Marsily, 1986) gives:

$$S_s = \rho_w g(\alpha + \beta_w \varphi) \approx \rho_w g \alpha = \frac{\rho_w g 3(1-2\nu)}{E} \tag{6}$$

where α is the solid phase compressibility, β_w is the fluid compressibility, and φ is the porosity. Setting $\rho_w = 1000$ kg.m^{-3}, g = 9.81 m.s^{-1}, ν = 0.2, with S_s ranging from 3.8 to 46.7 x10^{-5} m^{-1} gives a range for Young's modulus of 462 to 38 MPa (Table 6-3). Values obtained in this way are significantly lower than those derived from numerical interpretation of the data presented in Section 7, with the difference increasing as the test history progresses. One explanation for this response lies in the derivation of the parameters. The values of Young's modulus quoted above are based on analysis of the volumetric strain data, whereas in the modelling work (Section 7), most weight is placed on the flow rates which yield very poor fits to the net flow data. However, a problem in both analyses is the underlying assumption of linear elasticity when the specimen is probably behaving in a different way. Consequently the models in Section 7 are unable to fit all the data simultaneously, which suggests that the specimen is exhibiting some sort of visco-plastic deformation.

Upon completion of the test history the specimen was carefully removed from the apparatus (Figure 6-4) and its dimensions and mass recorded. Based on post-test estimates of specimen length and diameter (which are somewhat arbitrary given the irregular shape of the specimen) the data in Table 3-1 indicates the sample underwent a volumetric strain of around -1.5%. Based on this estimate, post-test measurements of saturation yield a value of around 108% indicating that the change in specimen volume has been significantly under-estimated. Analysis of the unload data in Table 6-1 confirms this hypothesis and yields a value for the cumulative volumetric strain of around –2.7%. When this parameter is used in the calculation of post-test saturation a value of approximately 100% is obtained. This corroborative observation strongly suggests that the volumetric strain derived by mass balance measurements during test stages [1] to [7] provides an accurate measure of the true system response.

Stage no.	Average effective stress (MPa)	Specific storage ($m^{-1} \times 10^5$)	Young's modulus (MPa)
2	3.14	17.3	102
3	2.51	3.8	462
4	1.86	6.3	279
5	1.22	8.6	204
6	0.59	16.6	106
7	0.40	46.7	38

Table 6-2 Estimates for specific storage and Young's modulus based on α values derived from the consolidation data.

Figure 6-4 Post-test photograph of the Opalinus Clay specimen. Upon decommissioning of the test, measurements of sample dimension clearly indicated an increase in specimen volume (i.e. swelling).

7 Numerical modelling

The finite element code STAFAN (INTERA, 1980), which models coupled porewater flow and elastic deformation, was used to model all stages of this test. Although this code has been modified to allow the boundary conditions to vary in magnitude with time, so that it is possible to accommodate the step changes in injection and confining pressures, it is not possible for boundary conditions to change type during the course of a simulation. In this test this occurs when the guard rings are isolated from the end piece filters, with the boundary conditions changing from specified porewater pressure (Dirichlet boundary conditions) to no-flow (Neumann boundary conditions). Initial modeling has been done with guard ring pressures set equal to end piece filter pressures throughout. This may be expected to lead to slightly under-estimating the specimen permeability.

7.1 MODELING ALL STAGES TOGETHER

The test specimen is modelled as an homogeneous material, and in the absence of useful data from the guard rings it has been necessary to assume isotropic permeability. The specimen porosity has been estimated separately to be 15%. The configuration of the experiment is such that it is not possible to uniquely determine both Young's modulus and Poisson's ratio, so separate models have been obtained with Poisson's ratio set to 0.15, 0.2, and 0.25. The permeability and Young's modulus were then adjusted to provide fits to the data.

As discussed above, greatest weight was given to data from the middle stages so that the permeability was determined by the requirement that the flow rate during the steady phases of those stages should be about 0.6 $\mu l.h^{-1}$, giving a permeability of 5.1×10^{-21} m^2. The value of the Young's modulus then determines the rate at which the inflow and outflow rate curves converge in each stage, and also the 'plateau' values in the net flow curve. Adjusting the value of Young's modulus to reproduce the net flow at around 90 days also gave a reasonable fit to the flow rate curves for the early and middle stages of the test. A value of 400 MPa was obtained with a Poisson's ratio of 0.2. Figures 7-1 and 7-2 show the fit of the model to the flow rate and net flow datasets respectively. Figures 7-3, 7-4, and 7-5 show more detailed plots of the comparison of the model output with the various stages of flow rate data.

Essentially identical fits to the data were obtained when setting Poisson's ratio to 0.15 and 0.25 by using values for Young's modulus of 467 and 333 MPa respectively. It may be noted that the solid phase compressibility, α, is given by (de Marsily, 1986)

$$\alpha = \frac{3(1-2\nu)}{E} \tag{7}$$

where ν is the Poisson's ratio and E is the Young's modulus. For all three fits given above, α has the value of 4.5×10^{-9} Pa^{-1}.

7.2 MODELING STAGES SEPARATELY

The modelling above sought a single consistent fit to the whole of the dataset with a single set of parameters. In this section individual stages of the test are examined and modelled separately. All models were run with Poisson's ratio set to 0.2.

7.2.1 Stages 1 and 2

Firstly, stages [1] and [2] are taken together as they differ from the other stages in that there is no change of confining pressure, just a change in the injection pressure. The model curves shown in Figures 7-6 and 7-7 were obtained from STAFAN using $k = 3.8 \times 10^{-21}$ m^2 and E = 290 MPa, giving $\alpha = 6.2 \times 10^{-9}$ Pa^{-1} by Equation (7). Good fits are obtained to both flow rate and net flow data.

7.2.2 Stage 3

The model curves shown in Figures 7-8 and 7-9 were obtained from STAFAN using $k = 4.3 \times 10^{-21}$ m^2 and E = 570 MPa, giving $\alpha = 3.2 \times 10^{-9}$ Pa^{-1} by Equation (7). A reasonable fit is obtained to the flow rate data, but the net flow data are poorly represented.

7.2.3 Stage 4

The model curves shown in Figures 7-10 and 7-11 were obtained from STAFAN using $k = 5.1 \times 10^{-21}$ m^2 and E = 370 MPa, giving $\alpha = 4.9 \times 10^{-9}$ Pa^{-1} by Equation (7). A reasonable fit is obtained to the flow rate data, but the net flow data are poorly represented.

7.2.4 Stage 5

The model curves shown in Figures 7-12 and 7-13 were obtained from STAFAN using $k = 5.1 \times 10^{-21}$ m^2 and E = 310 MPa, giving $\alpha = 5.8 \times 10^{-9}$ Pa^{-1} by Equation (7). A good fit is obtained to the flow rate data, but the net flow data are poorly represented.

7.2.5 Stage 6

The model curves shown in Figures 7-14 and 7-15 were obtained from STAFAN using $k = 7.5 \times 10^{-21}$ m^2 and E = 240 MPa, giving $\alpha = 7.5 \times 10^{-9}$ Pa^{-1} by Equation (7). A reasonable fit is obtained to the flow rate data, but the net flow data are poorly represented.

7.2.6 Stage 7

The model curves shown in Figures 7-16 and 7-17 were obtained from STAFAN using $k = 9.5 \times 10^{-21}$ m^2 and E = 240 MPa, giving $\alpha = 7.5 \times 10^{-9}$ Pa^{-1} by Equation (7). A reasonable fit is obtained to the inflow rate data, but the outflow rate and net flow data are poorly represented.

It may be noted that the choice of Young's modulus for this model was determined primarily to fit the transient variation of the inflow rate rather than the magnitude of the change of the net flow during the stage. In order to match the magnitude of the change in the net flow during the stage it is necessary to reduce the value of Young's modulus to 65 MPa, but even then the shape of the model net flow curve is a poor fit to the data, since it rises much faster and reaches a plateau by about 30 days. The transient phase of the flow rate data is also poorly represented by this model.

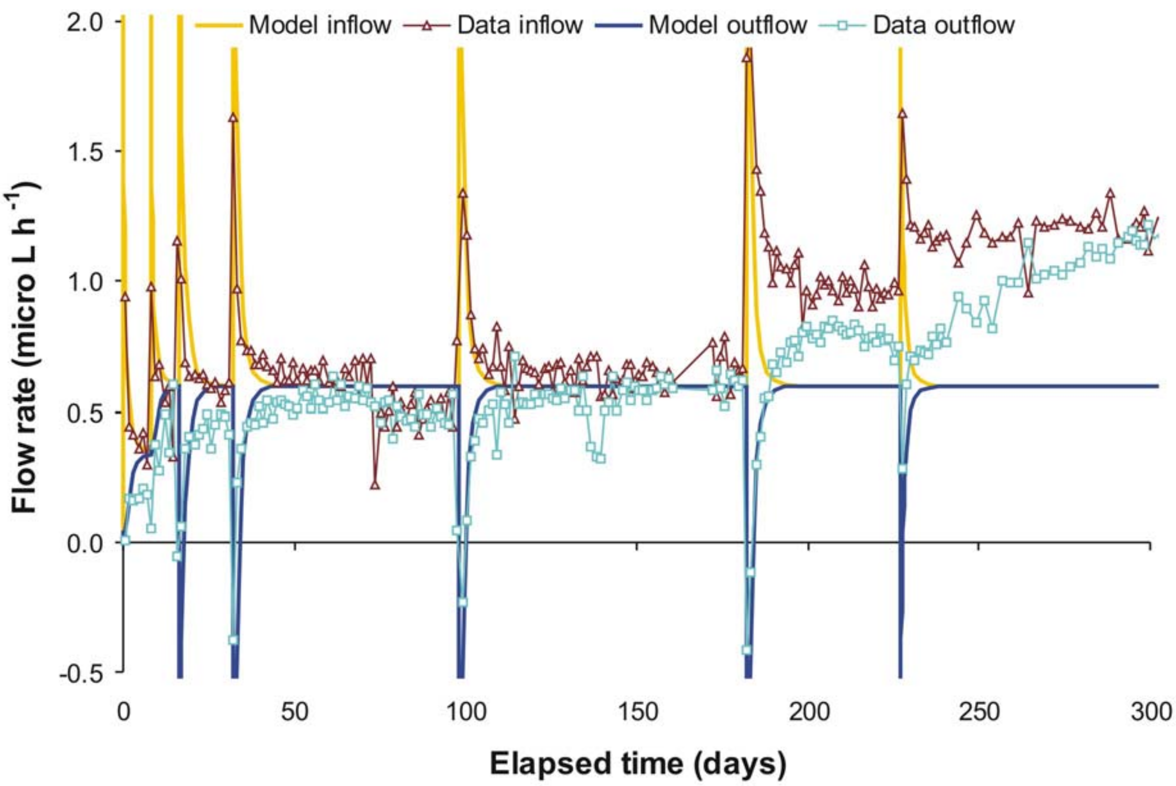

Figure 7-1 Comparison of model output with inflow and outflow data from the test.

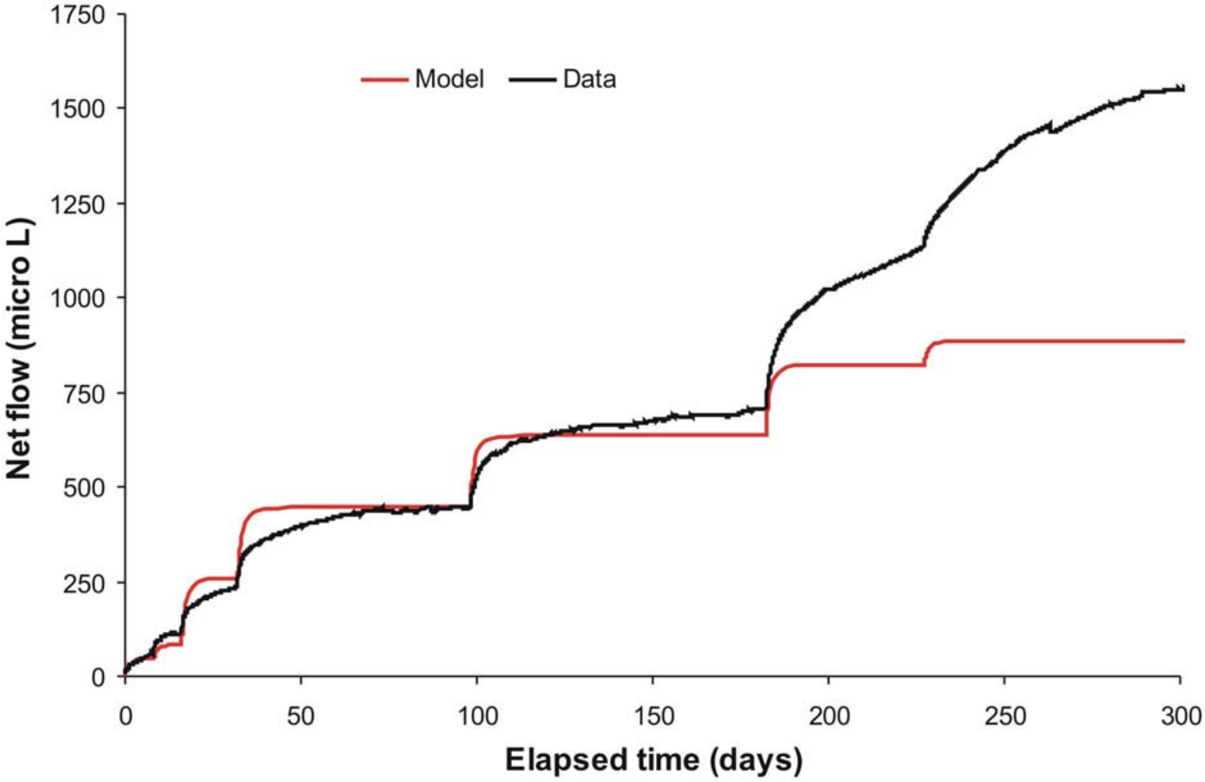

Figure 7-2 Comparison of model output with net flow data from the test.

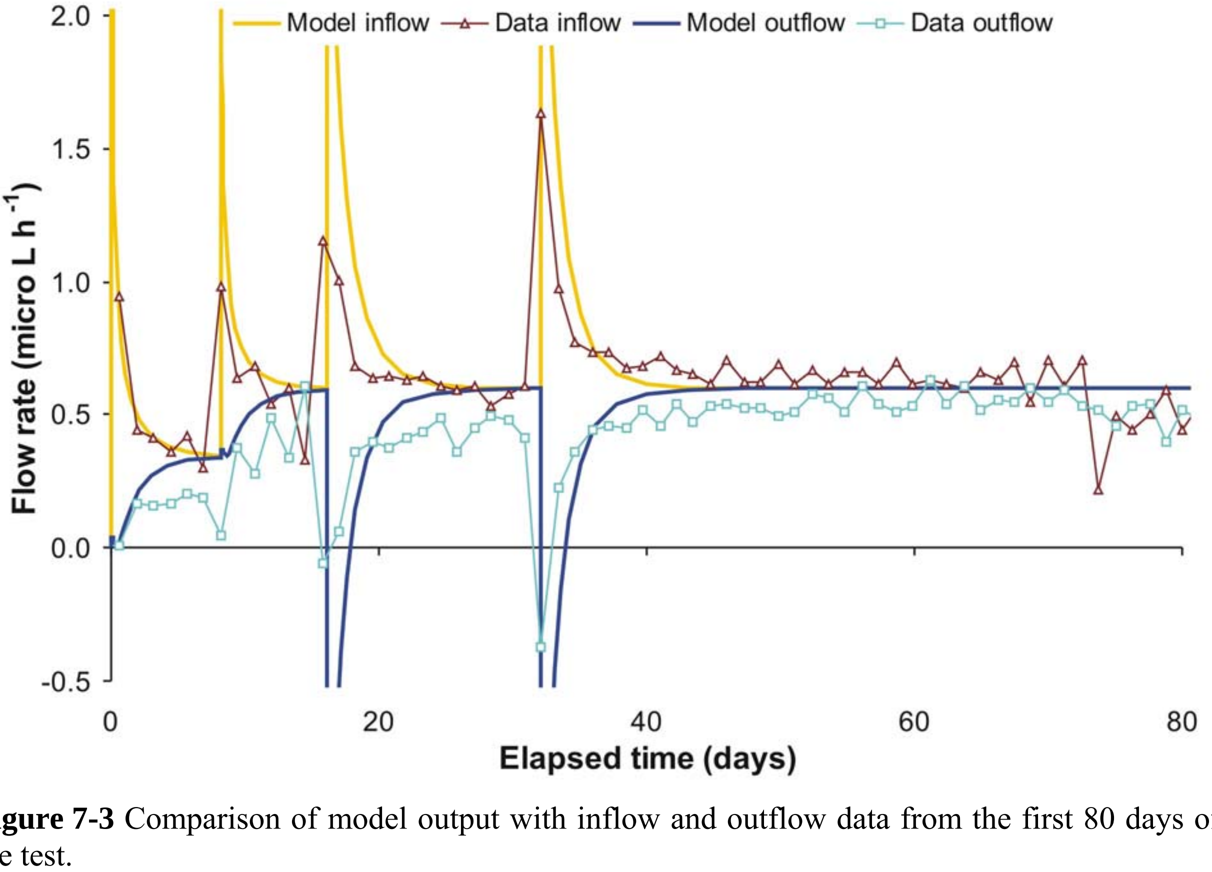

Figure 7-3 Comparison of model output with inflow and outflow data from the first 80 days of the test.

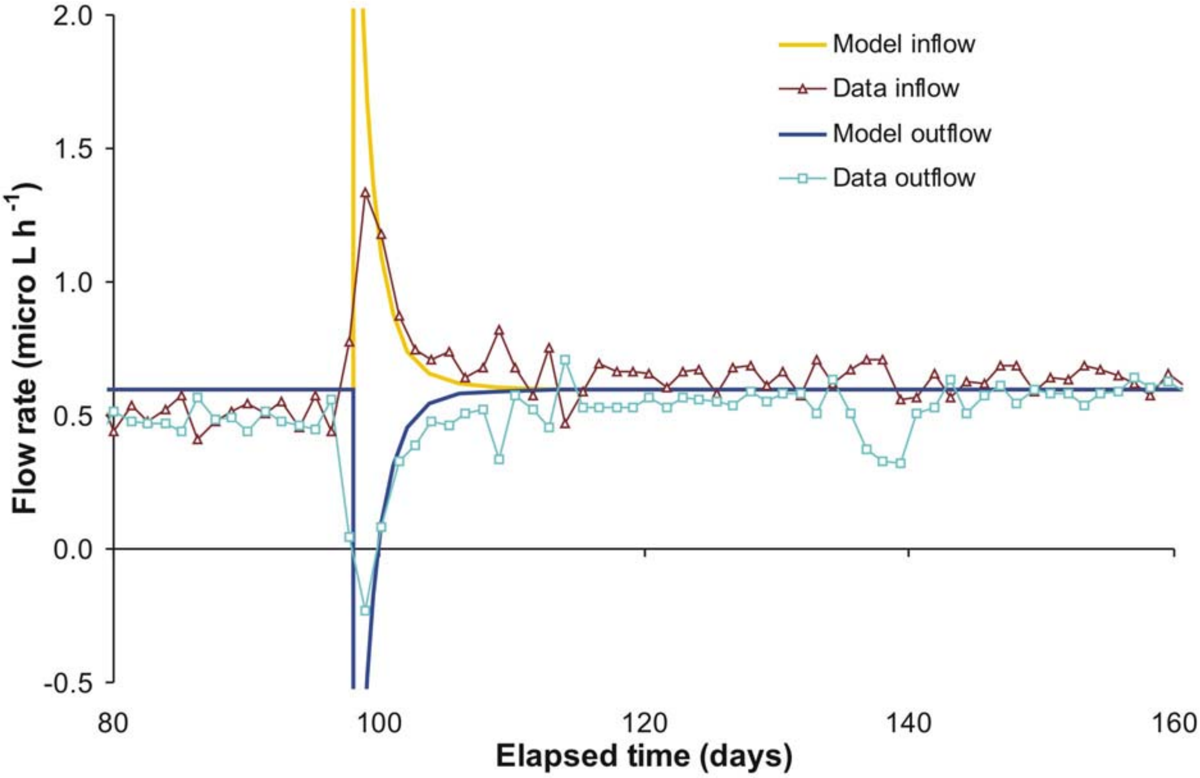

Figure 7-4 Comparison of model output with inflow and outflow data from days 80 to 160 of the test.

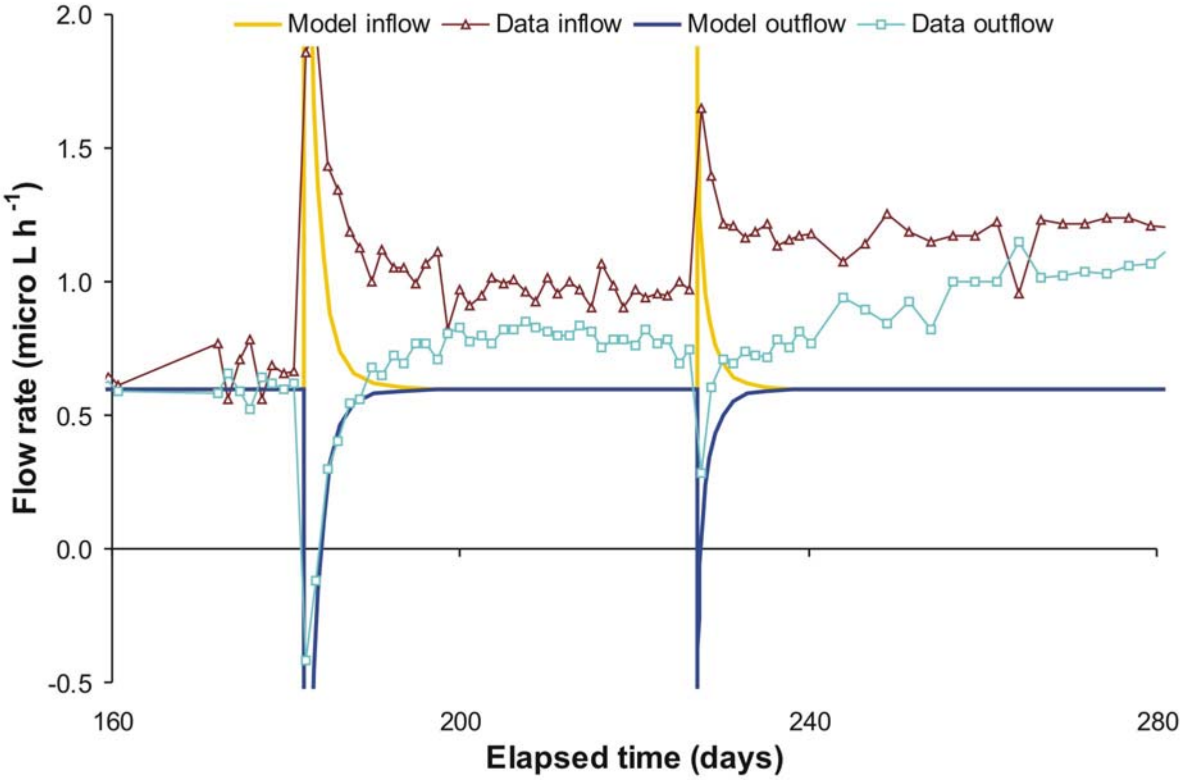

Figure 7-5 Comparison of model output with inflow and outflow data from days 160 to 280 of the test.

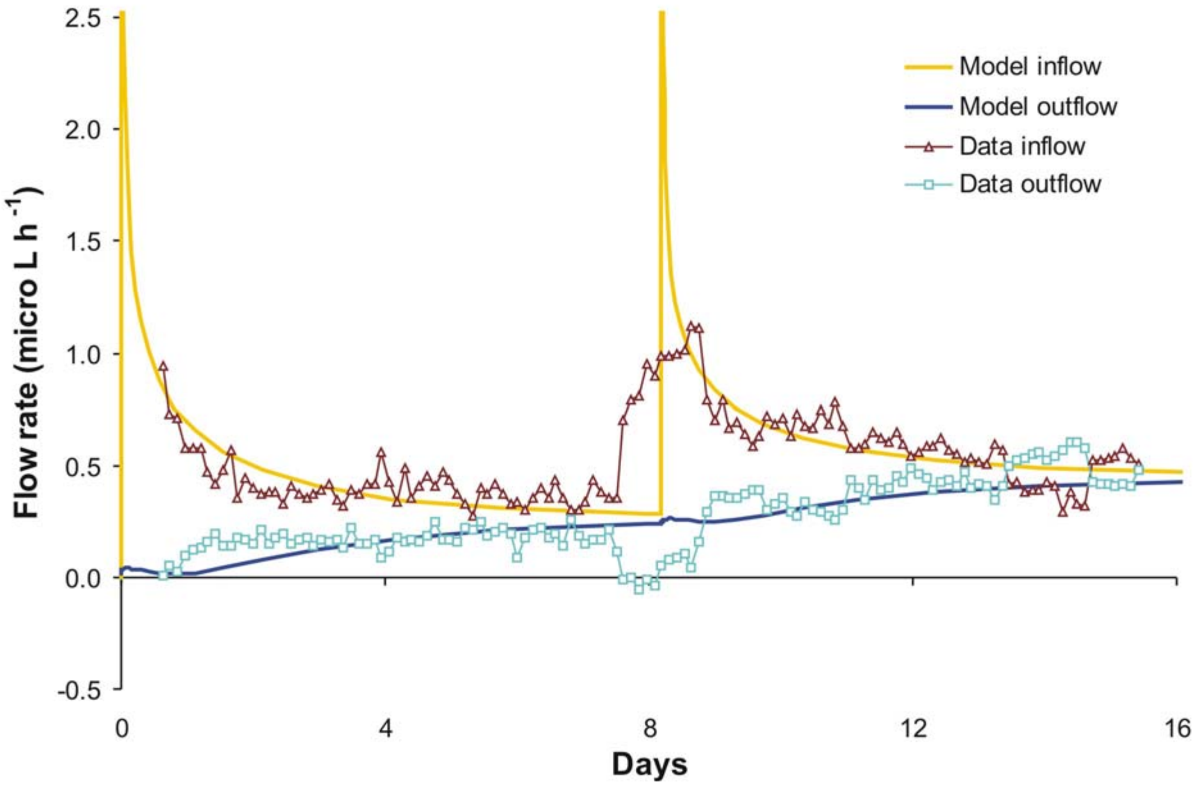

Figure 7-6 Comparison of model output with inflow and outflow data from stages [1] and [2] of the test.

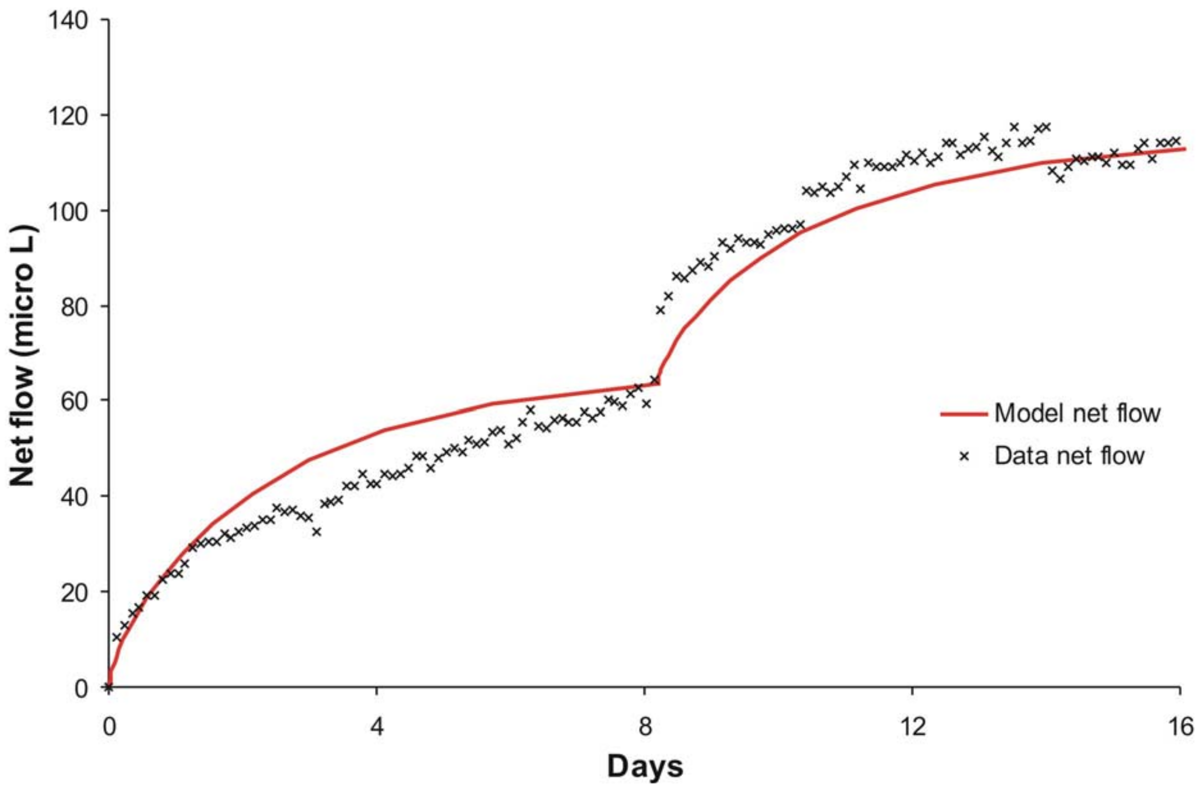

Figure 7-7 Comparison of model output with net flow data from stages [1] and [2] of the test.

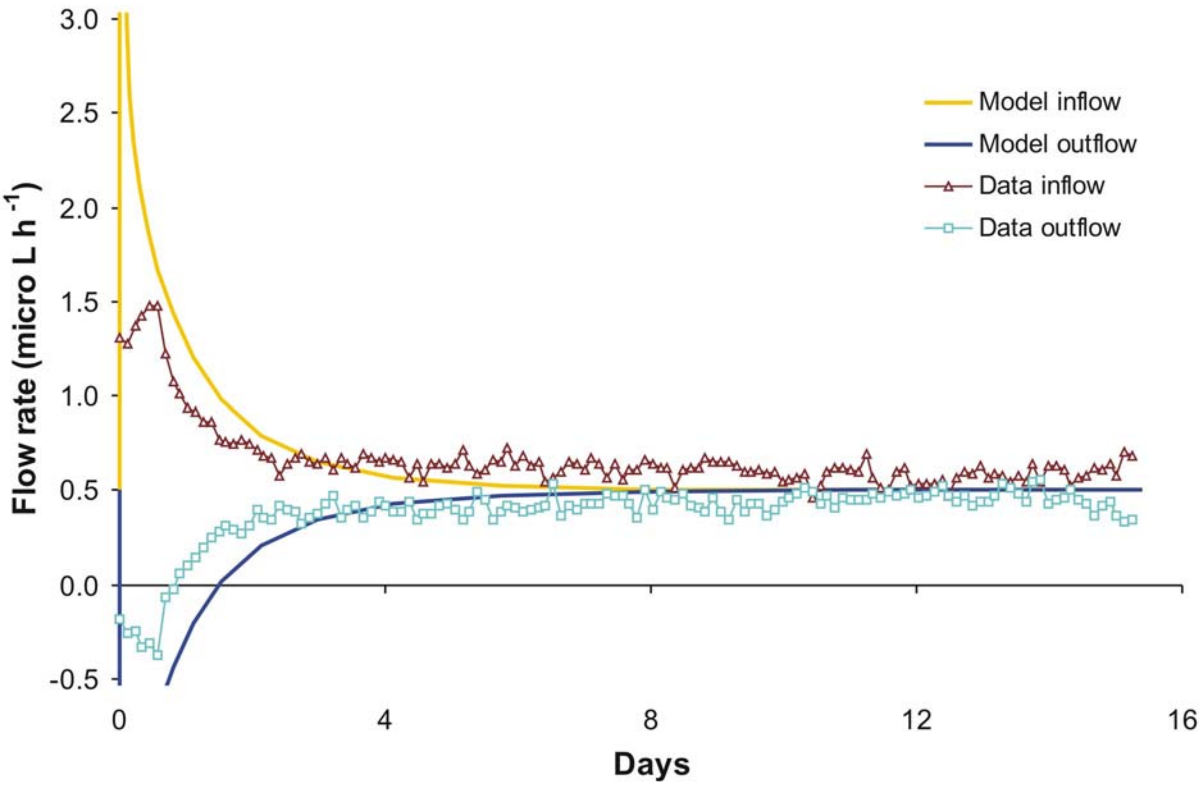

Figure 7-8 Comparison of model output with inflow and outflow data from stage [3] of the test.

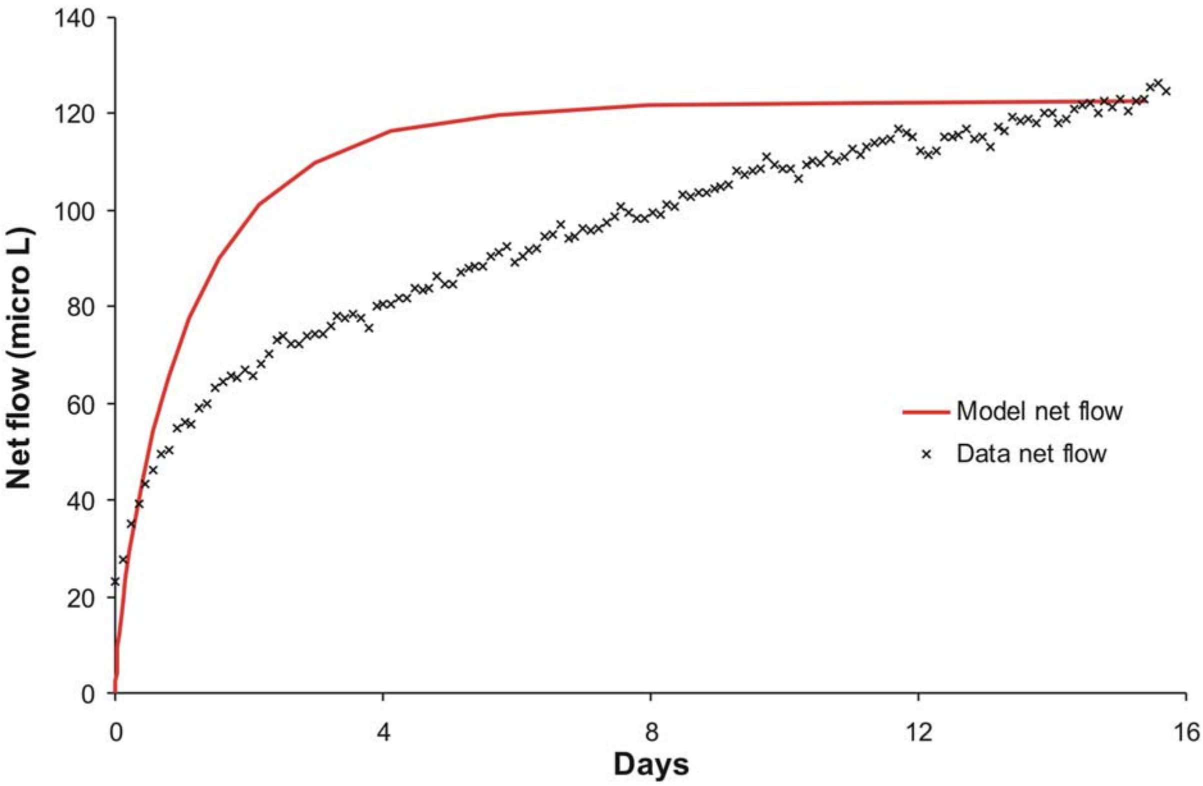

Figure 7-9 Comparison of model output with net flow data from stage [3] of the test.

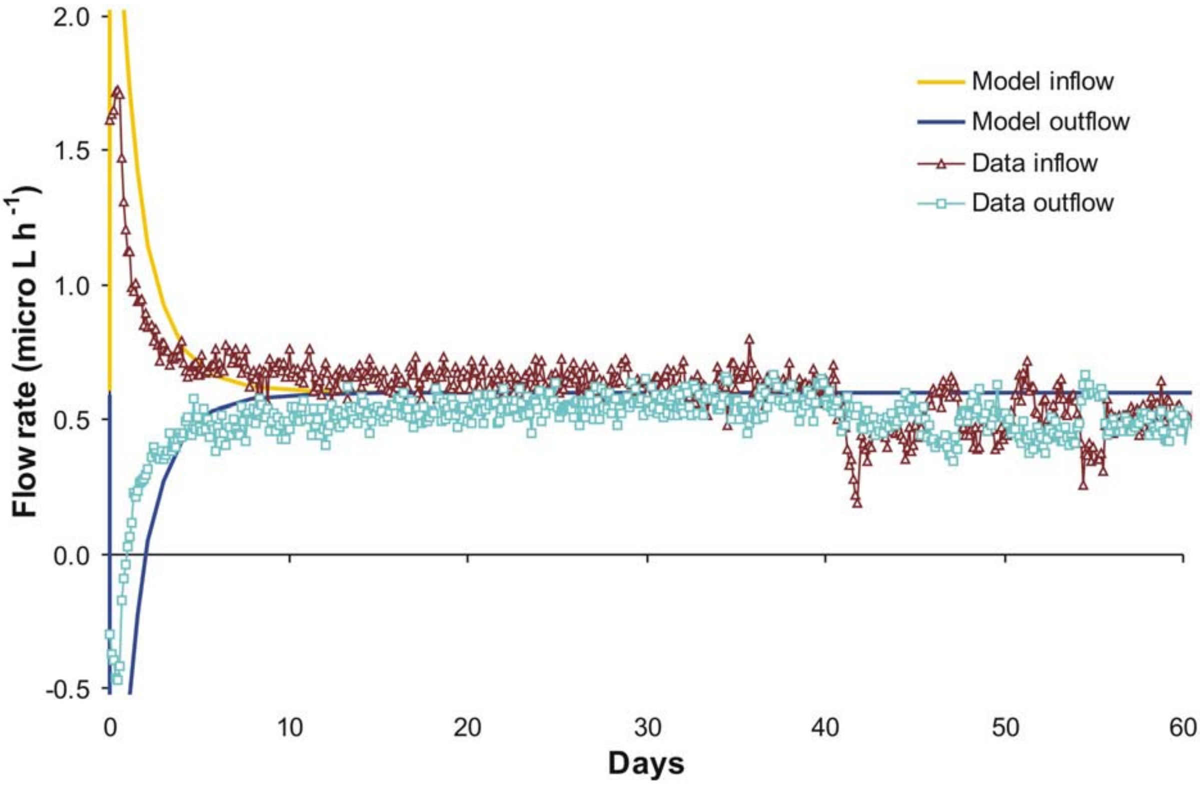

Figure 7-10 Comparison of model output with inflow and outflow data from stage [4] of the test.

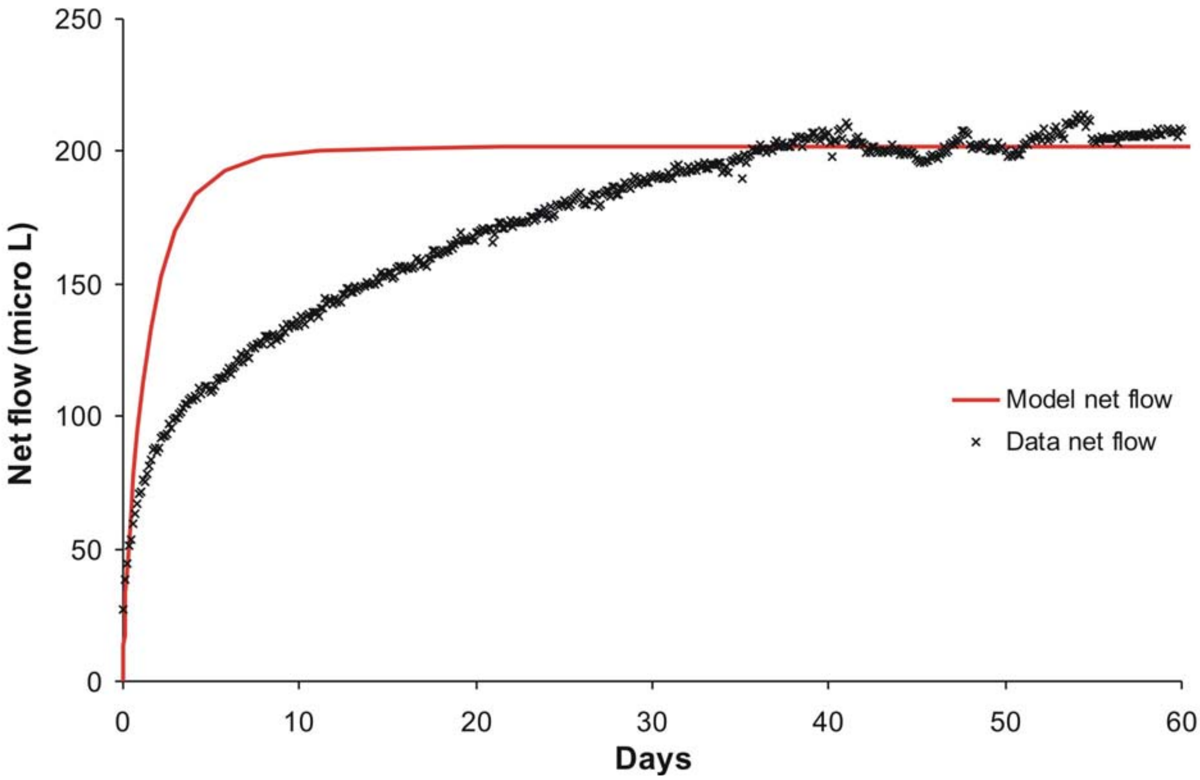

Figure 7-11 Comparison of model output with net flow data from stage [4] of the test.

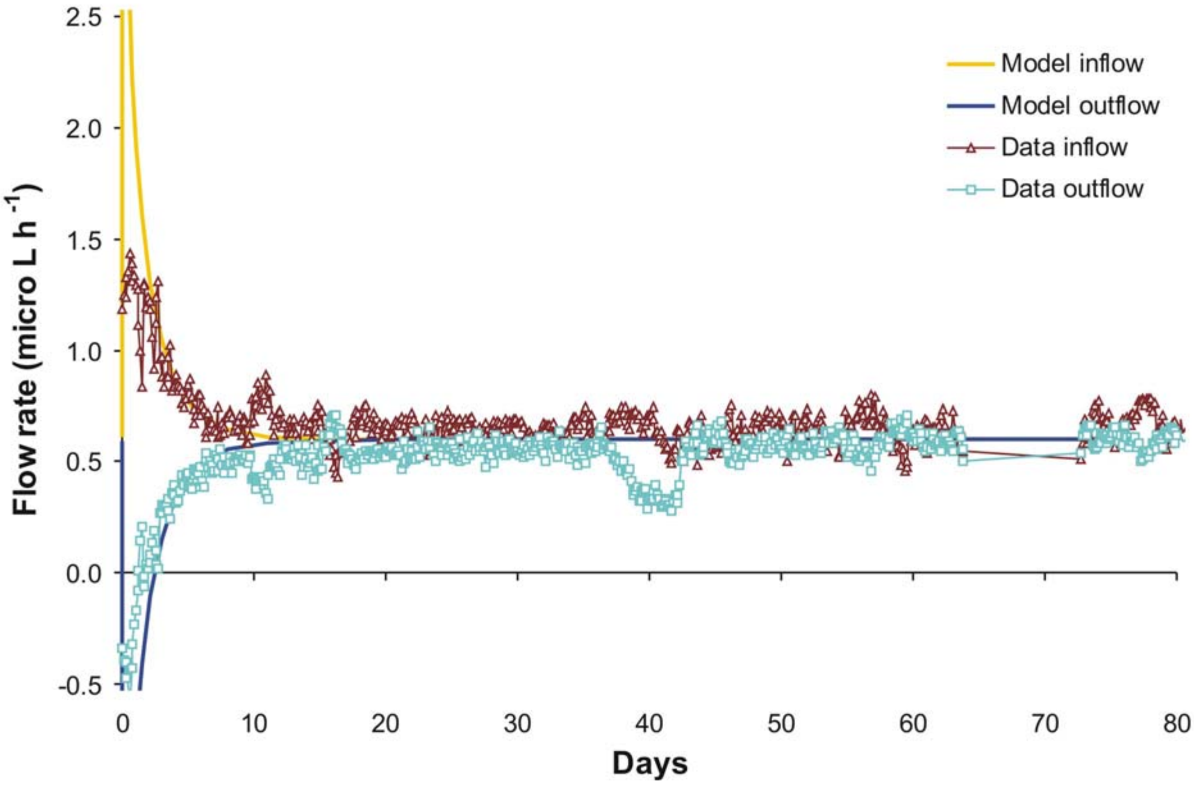

Figure 7-12 Comparison of model output with inflow and outflow data from stage [5] of the test.

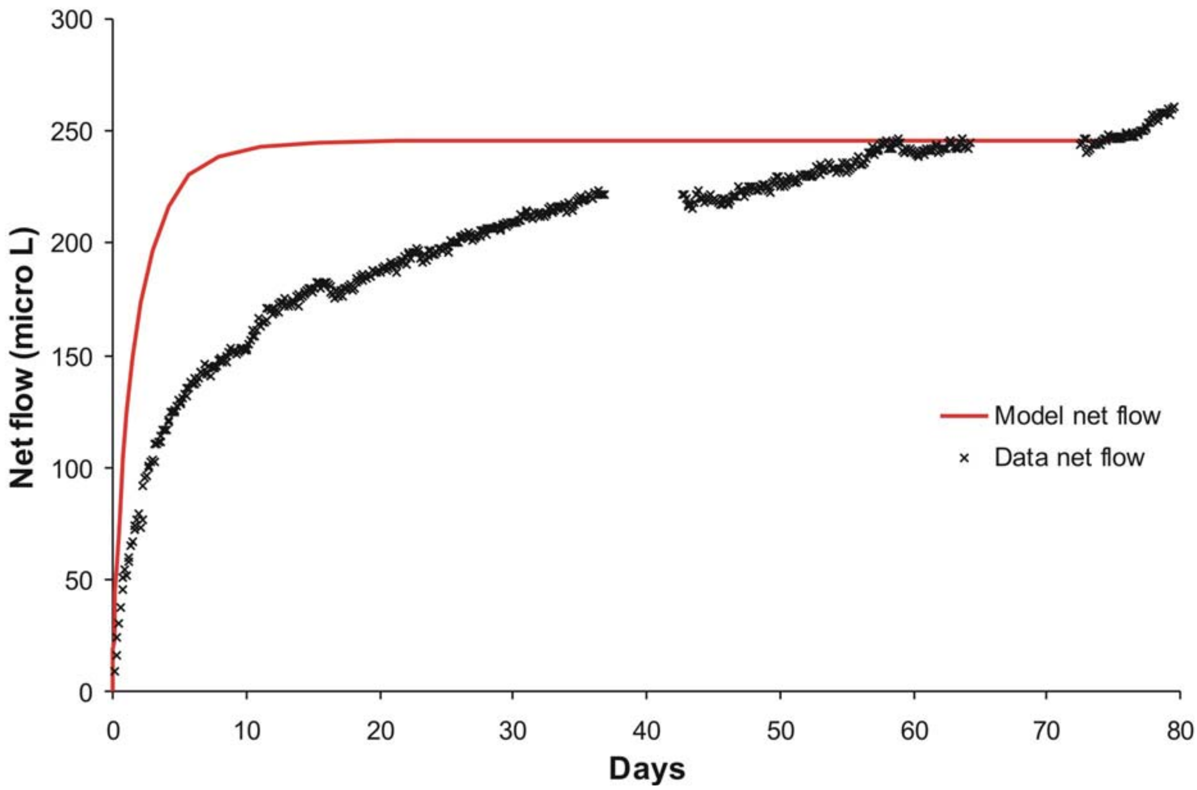

Figure 7-13 Comparison of model output with net flow data from stage [5] of the test.

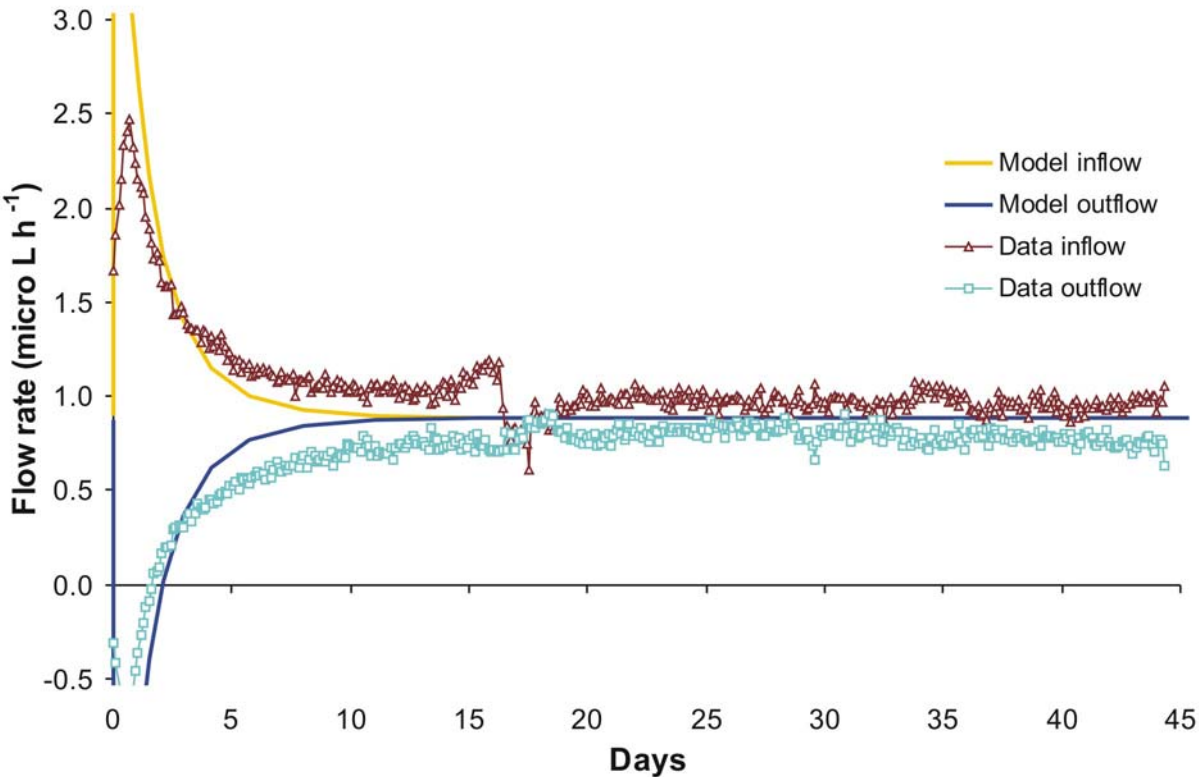

Figure 7-14 Comparison of model output with inflow and outflow data from stage [6] of the test.

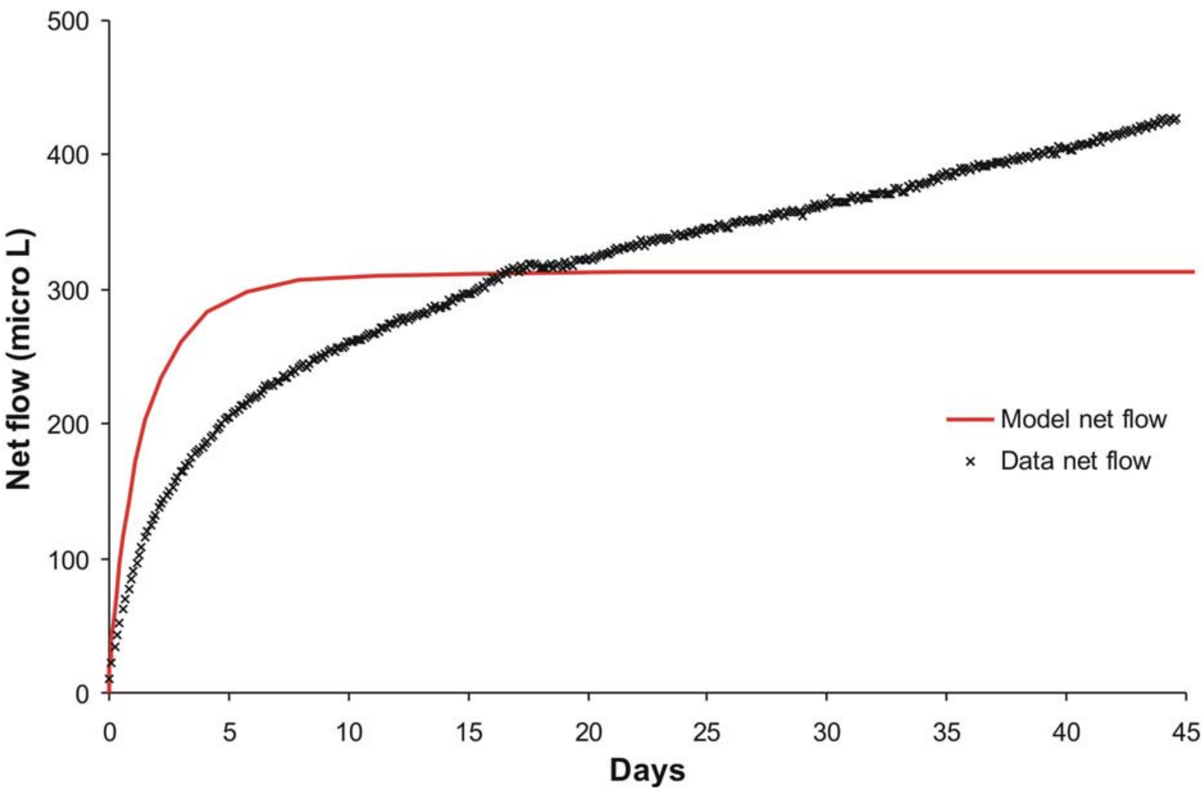

Figure 7-15 Comparison of model output with net flow data from stage [6] of the test.

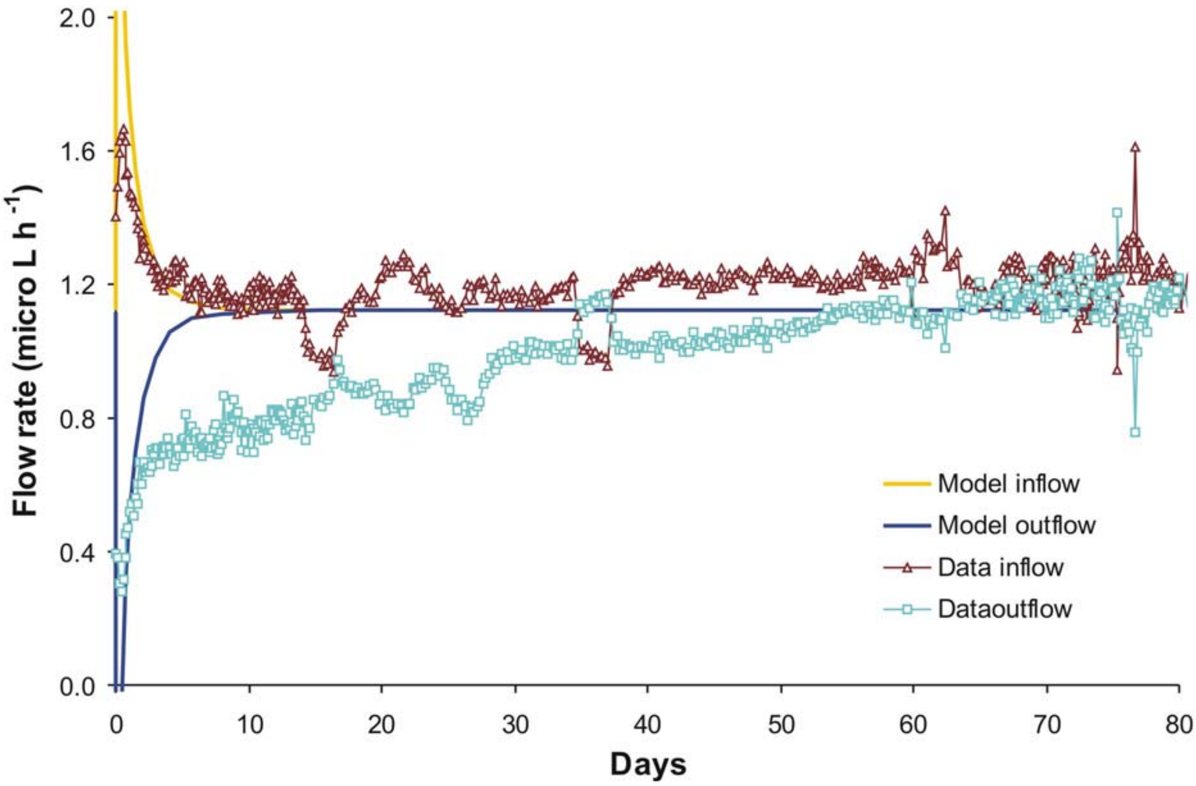

Figure 7-16 Comparison of model output with inflow and outflow data from stage [7] of the test.

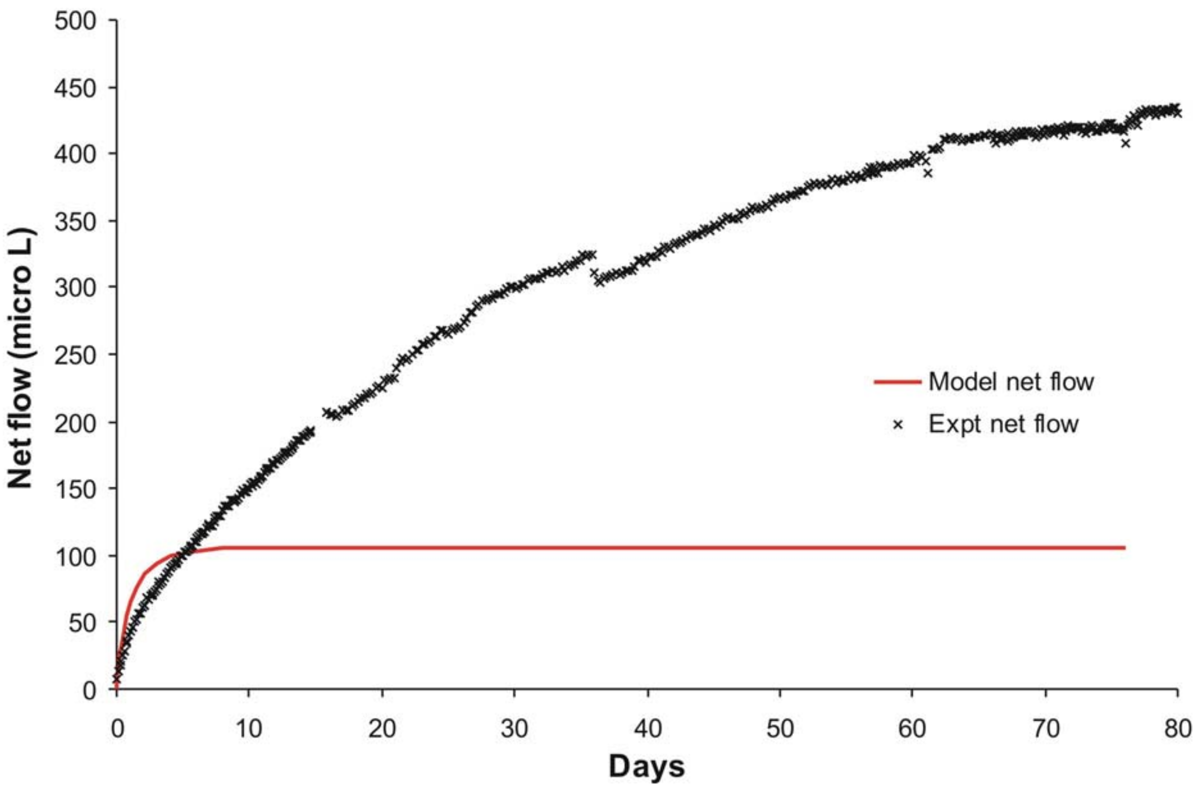

Figure 7-17 Comparison of model output with net flow data from stage [7] of the test.

7.2.7 Summary

The parameter values obtained from these models are collected in Table 7-1. It can be seen that permeability increases throughout the test, though with relatively little change over stages [1] to [5], and the Young's modulus declines after the first two stages. The compressibility follows the Young's modulus through Equation 7.

Stage no.	Permeability, k (m^2)	Young's modulus, E (MPa)	Compressibility, α (Pa^{-1})
1 and 2	3.8×10^{-21}	290	6.2×10^{-9}
3	4.3×10^{-21}	570	3.2×10^{-9}
4	5.1×10^{-21}	370	4.9×10^{-9}
5	5.1×10^{-21}	310	5.8×10^{-9}
6	7.5×10^{-21}	240	7.5×10^{-9}
7	9.5×10^{-21}	240	7.5×10^{-9}

Table 7-1 Summary of parameters from model fits.

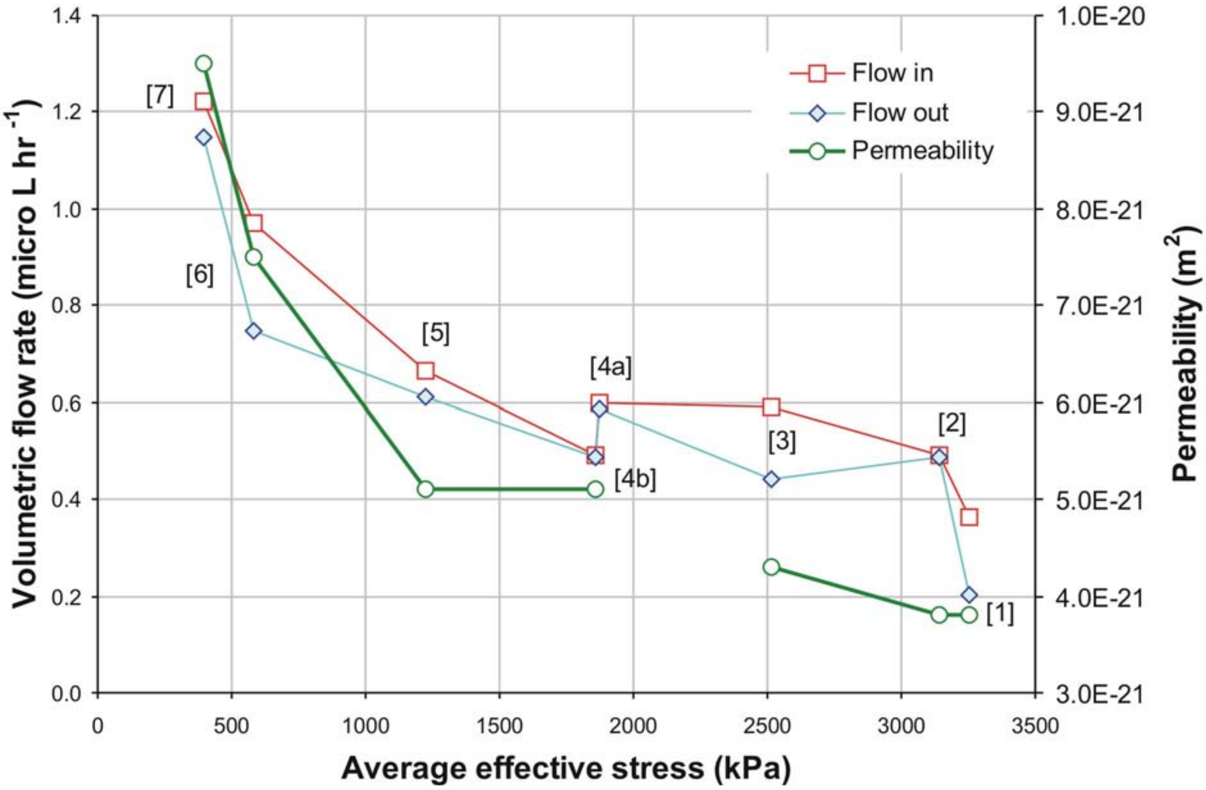

Figure 7-18 Cross-plot of volumetric flow rate and steady-state permeability against average effective stress for test stages [1] to [7] inclusive.

The data in Table 7-1 indicates permeability ranges from around 3.8 to 9.5 x 10^{-21} m^2 at average effective stresses of 3.25 and 0.40 MPa respectively. Cross-plotting volumetric flow rate and permeability data for each test stage against the average effective stress (Figure 7-18) clearly shows an increase in both parameters from test stage [5] onwards when average effective stress declines to below 1000 kPa. This may be caused by the development of an interconnected network of dilatant cracks at a critical value of effective stress.

8 Conclusions

Isotropic effective stress was reduced in a step wise manner (7 steps) on a specimen of Opalinus Clay subject to a constant hydraulic gradient. Based on these experiments, permeability values were found to be in the range 3.8 to 9.5×10^{-21} m^2 at average effective stresses of 3.25 to 0.40 MPa respectively. While a few of the test stages did not approach a well defined asymptote the data exhibits a significant increase in permeability when effective stress declined below around 1000 kPa. These may be associated with the development of an interconnected network of dilatant cracks as effective stress declines to some critical value, which may also explain the low modulus values noted in the study.

A plot of void ratio against logarithm of effective stress is sensibly linear for the test history showing that the specimen exhibits soil-like behaviour. Evidence suggests that the locus in void ratio-effective stress space corresponds to the rebound-reconsolidation line of theoretical soil mechanics. The general trend of increasing material compressibility and decreasing bulk modulus are also symptomatic of an increase in specimen volume due to swelling of the clay during stress unloading. The values of bulk modulus (derived during stress reduction) are small and can be explained by non-elastic deformation (e.g. swelling).

Storage values for the stress regime imposed during this study were found to range from 3.8 to 46.7×10^{-5} m^{-1}, exhibiting a general trend of increasing storage with decreasing effective stress. These values are significantly larger than those reported by Horseman et al. (2005). However, this can be explained by the stress dependency of the storage parameter.

Alpha values from this study are in general agreement to those obtained by Horseman et al. (2005) for clay in the overconsolidated domain, suggesting quantitatively similar material behaviour. Mass balance calculations indicate the amount of volumetric strain (swelling) per stage appears to increase as effective stress declines. Values of Young's modulus based on analysis of the unloading data are generally lower than those derived from numerical modelling of the data. However, both determinants exhibit a general decreasing trend as average effective stress declines.

The combination of low modulus values and the inability of the numerical model to fit all the data simultaneously, strongly suggests that the specimen is exhibiting a form of visco-plastic deformation during the unloading process.

However, data from this study clearly shows that on the scale of this experiment, the specimen continues to exhibit exceptionally low permeability even when subject to very small isotropic effective stresses (equivalent to exhumation of the clay to a depth of around 20m).

It is worth noting that the general literature lacks information on system responses during unloading and that elasticity theory is primarily concerned with material deformation during loading. The issue of hysteresis in such systems is complex and poorly understood.

References

The British Geological Survey holds most of the references listed below, and copies may be obtained via the library service subject to copyright legislation (contact libuser@bgs.ac.uk for details). The library catalogue is available at: http://geolib.bgs.ac.uk.

ATKINSON, J H. and BRANSBY, P L. 1978. The Mechanics of Soils: An Introduction to Critical State Soil Mechanics. McGraw-Hill, New York.

GAUTSCHI, A. 2001. Hydrogeology of a fractured shale (Opalinus Clay): Implications for deep geological disposal of radioactive wastes. *Hydrogeology Journal*, Vol. 9, pp 97-107, Springer-Berlin, Heidelberg.

HORSEMAN, S T. 2001. Self-healing of fractures in argillaceous media from the geomechanical point of view. In: Proceedings of a Topical Session on Self-healing held in Nancy, France. IGSC Working Group on Measurement and Physical Understanding of Groundwater Flow Through Argillaceous Media. OECD/NEA Radioactive Waste Management Committee. NEA/RWM/CLAYCLUB(2001)5 (unclassified).

HORSEMAN, S T, HARRINGTON, J F AND NOY, D J. 2007. Swelling and osmotic flow in a potential host rock. *Physics and chemistry of the Earth*, Vol. 32, pp 408-420.

HORSEMAN, S T, HARRINGTON, J F, BIRCHALL, D J, NOY, D J AND CUSS, R J. 2005. Consolidation and rebound properties of Opalinus clay: A long-term, fully-drained test. Commissioned Report CR/05/128 (Commercial - In Confidence). *British Geological Survey*, Environmental Protection Programme.

HORSEMAN, S T AND HARRINGTON, J F. 1994. Migration of repository gases in an overconsolidated clay. *British Geological Survey*, British Geological Survey, Technical report WE/94/7.

HORSEMAN, S T, WINTER, M G and ENTWISLE, D C. 1993. Triaxial experiments on Boom Clay. In: *The Engineering Geology of Weak Rock*, Cripps, J.C. et al., (eds), Balkema, Rotterdam, 36-43.

HUYAKORN, P S AND PINDER, G F. 1983. Computational Methods in Subsurface Flow. Academic Press, New York, 473 pp.

INTERA ENVIRONMENTAL CONSULTANTS INC. 1983. STAFAN: A Two-Dimensional Code for Fluid Flow and the Interaction of Fluid Pressure and Stress in Fractured Rock for Repository Performance Assessment. Office of Nuclear Waste Isolation Report ONWI 427.

MARSILY, G de. 1986. Quantitative Hydrogeology for Engineers, Academic Press, San Diego, 440 p.

PEARSON, F J, SCHOLTIS, A, GAUTSCHI, A, BAEYANS, B, BRADBURY, M and DEGUELDRE, C. 1999. Section 6.2 - Chemistry of porewater, In: Mont Terri Rock Laboratory: Results of the Hydrogeological, Geochemical and Geotechnical Experiments Performed in 1996 and 1997. Thury, M. and Bossart, P. (eds), Geological Report 23, pp 129-147, The Swiss National Hydrological and Geological Survey, CH-3003, Bern, Switzerland.

SCHOFIELD, A and WROTH, P W. 1968. Critical State Soil Mechanics. McGraw-Hill, London.

WOOD, D M. 1990. Soil Behaviour and Critical State Soil Mechanics. Cambridge University Press, 462 pp.